universität wien

MASTERARBEIT / MASTER'S THESIS

Titel der Masterarbeit / Title of the Master's Thesis

„Synthesis of Hydrophilic Core-Shell Superparamagnetic Iron Oxide Nanoparticles“

verfasst von / submitted by

Alemeh Karami

angestrebter akademischer Grad / in partial fulfilment of the requirements for the degree of

Master of Science (MSc)

Wien, 2020 / Vienna 2020

Studienkennzahl lt. Studienblatt / degree programme code as it appears on the student record sheet:	UA 066 299
Studienrichtung lt. Studienblatt / degree programme as it appears on the student record sheet:	Interdisziplinäres Masterstudium Environmental Sciences
Betreut von / Supervisor:	Univ. Prof. Dr. Thilo Hofmann

Acknowledgment

I would like to pay my special regards to Prof. Eric Reimhult for hosting me in his research group, providing me with all the necessary facilities, guiding and supervising

I wish to express my gratitude to my advisor Dr. Behzad Shirmardi for imparting his knowledge and expertise in this study.

The physical and technical contribution of “Institute for Biologically Inspired Material, Department of Nanobiotechnology, University of Natural Resources and Life Sciences of Vienna” is truly appreciated. Without their support and funding, this project could not have reached its goal.

I would also like to acknowledge Prof. Thilo Hofmann for allowing me to graduate under his official supervision and reading my thesis.

My thanks and appreciation also go to my colleagues and people whose assistance was a milestone in the completion of this project.

Last but not the least, I must express my very profound gratitude to my family and to my spouse for providing me with unfailing support and continuous encouragement throughout my years of study and through the process of researching and writing this thesis. This accomplishment would not have been possible without them. Thank you.

Abstract

Uniform spherical superparamagnetic iron oxide nanoparticles (SPIONs) with narrow size distribution have been synthesised by thermal decomposition of iron pentacarbonyl and iron oleate. These nanoparticles are originally capped with a shell of hydrophobic oleate. Superparamagnetic iron oxide nanoparticles can be applied as contrasting agents in medicine. For this application, they have to be covered with a dense shell of biocompatible and hydrophilic ligands to prevent them from aggregation, uptake by cells, and recognition by the immune system. Thus, the oleate shell must be completely replaced by hydrophilic ligands. Ligand stripping and sequential regrafting is an approach to achieve this and provide superparamagnetic iron oxide nanoparticles with colloidal stability in biological media. The next challenge after replacing the polymer ligand on the nanoparticle surface is efficiently removing extra unbound ligand and displaced initial oleic acid from the reaction solution. In this study, I investigated the grafting of polyethylene glycol (PEG-5000) anchored with nitrodopamine on different SPION sizes from 6.1 to 20.7 nm. Additionally, I used dialysis, magnetic decantation and membrane centrifugation methods to purify the dispersion from excess free PEG. TEM graphs revealed that nanoparticles are uniformly sized and shaped. PEG grafting densities calculated from thermogravimetric analysis of organic mass loss during thermal decomposition indicated grafting densities between 0.5-6 chains/nm^2. Grafting densities around 1 chain/nm^2 are considered promising results with respect to colloidal stability in biological media. SPIONs with optimal grafting densities showed colloidal stability through DLS measurement over 40 days of monitoring. Full ligand replacement was proved by ^{1}H-NMR experiment.

Key words: Synthesis, Superparamagnetic iron oxide nanoparticle (SPIONs), hydrophilic shell, Polyethyleneglycol (PEG)

Kurzfassung

Einheitliche sphärische superparamagnetische Eisenoxid-Nanopartikel (SPIONs) mit enger Größenverteilung wurden durch thermische Zersetzung von Eisenpentacarbonyl und Eisenoleat synthetisiert. Diese Nanopartikel sind ursprünglich mit einer Hülle aus hydrophobem Oleat bedeckt. Superparamagnetische Eisenoxid-Nanopartikel können als Kontrastmittel in der Medizin eingesetzt werden. Für diese Anwendung müssen sie mit einer dichten Hülle aus biokompatiblen und hydrophilen Liganden bedeckt werden, damit sie nicht aggregieren, von den Zellen aufgenommen und vom Immunsystem erkannt werden können. Die Oleatschale muss daher vollständig durch hydrophile Liganden ersetzt werden. Liganden-Stripping und sequenzielles Refrafteding ist ein Ansatz, um dies zu erreichen und superparamagnetischen Eisenoxid-Nanopartikeln in biologischen Medien kolloidale Stabilität zu verleihen. Die nächste Herausforderung nach dem Ersetzen des Polymerliganden auf der Oberfläche der Nanopartikel ist die effiziente Entfernung des zusätzlichen ungebundenen Liganden und der verdrängten anfänglichen Ölsäure aus der Reaktionslösung. In dieser Studie untersuchte ich die Pfropfung von mit Nitrodopamin verankertem Polyethylenglykol (PEG-5000) auf verschiedene SPION-Grössen von 6.1 bis 20.7 nm. Zusätzlich verwendete ich Dialyse-, Magnetdekantier- und Membranzentrifugationsmethoden, um die Dispersion von extra freiem PEG zu reinigen. TEM-Diagramme zeigten, dass die Nanopartikel eine einheitliche Größe und Form haben. Die aus den TGA-Massenverlustergebnissen berechneten PEG-Pfropfungsdichten zeigten, dass die Pfropfungsdichten zwischen 0.5-6 Ketten/nm^2 liegen. Pfropfdichten um 1 Kette/nm^2 gelten als vielversprechende Ergebnisse in Bezug auf die kolloidale Stabilität in biologischen Medien. SPIONs mit optimalen Pfropfdichten zeigten kolloidale Stabilität durch DLS-Messung über 40 Tage Monitoring. Vollständiger Ligandenersatz wurde durch ^{1}H-NMR-Experiment nachgewiesen.

Schlagwörter: Synthese, Superparamagnetische Eisenoxid-Nanopartikel (SPIONs), hydrophile Schale, Polyethylenglykol (PEG)

Table of Contents

List of figures

List of tables

List of abbrevations

NP	Nanoparticle
SPION	Superparamagnetic iron oxide nanoparticle
nm	Nanometer
PEG	Poly ethelyn glycol
NDA	Nitrodopamine
TEM	Transmission electron microscope
DLS	Dynamic light scattering
TGA	Thermogravimetric analysis
COMU	(1-Cyano-2-ethoxy-2-oxoethylidenaminooxy) dimethylamino-morpholino-carbenium hexafluorophosphate
CA	Contrast agent
GBCA	Gadolinium based contrast agents
NMR	Nuclear magnetic resonance
MRI	Magnetic resonance imaging
DMF	Dimethylformamide
PBS	Phosphate buffered saline
BSA	Bovine serum albumin
MWCO	Molecular weight cut-off

1. Introduction

Nanoparticles are common and widespread compounds present in daily life products and occur ubiquitously in the environment. According to the International Standardization Organisation (ISO) a nanoparticle is a discrete piece of material in which all external dimensions are in the range of approximately 1 nm to 100 nm.[1]

The increase in surface area to volume ratio in nanoparticles compared to their respective bulk counterparts results in dissimilar physical and chemical characteristics such as higher reactivity, lower melting point, changes in geometric structure, optical and magnetic properties. Novel and beneficial properties of nanomaterials have led to a significant increase in nanotechnology research and product development during recent decades. These new nanoproducts provide solutions to current problems but also generate concerns about their health and environmental effects, which require further research and investigation.[2]

Basically, nanoparticles can be natural, manufactured or incidental. Natural nanoparticles are organic and inorganic compounds in nanoscale occurring from biological and geological sources and have been forming on the planet for millions of years. Examples of natural nanoparticles are iron, manganese and aluminium oxides and hydroxides, alumina silicates and humic substances.[1, 3, 4] Manufactured or engineered nanoparticles are intentionally produced to have selected properties or composition. Engineered nanoparticles are widely used in industrial, commercial and in-home products, such as Ag[5], SiO_2[6], TiO_2[7] and CeO_2[8]. Incidental nanoparticles are produced as an unintentional by-product of processes like combustion, volcanic eruption, mineral weathering and corrosion of pipelines.[9]

Iron oxide nanoparticles are a diversified group of nanomaterial which have been a topic for intensive and widespread research due to their abundance in nature, being non-costly and non-toxic in the first place. Iron oxide nanoparticles are either natural or engineered. Formation of nanoparticulated iron oxides in the environment is favored by the elemental abundance of iron, oxygen and hydrogen. Diverse natural occurring nanostructures of iron oxides and oxyhydroxides are formed and resided in different parts of the ecosystem and play an important role in many biogeochemical processes. These compounds have been estimated to weigh 10^5 Tg in soils.[10, 11] Iron oxide nanoparticles in the environment undergo chemical and physical reactions such as redox, precipitation, adsorption, complexation, aggregation and photochemical reactions when they are in contact with organic or inorganic ligands. These reactions can result in changes in their physicochemical properties.[12-14] The engineered iron oxide nanoparticles have been exploited in a vast

variety of applications including industrial applications such as magnetic inks,[15] magnetic recording media,[16] magnetic absorbent,[17, 18] catalysts,[19] ferrofluids,[20] application in medicine such as contrast agents for imaging and diagnosis,[21-27] therapeutic agents for cancer treatment,[21-29] drug delivery vehicles,[30, 31] environmental applications such as remediating soils polluted with arsenic, PCBs and other organic and inorganic pollutants[32, 33] and many other applications and technological products. In recent decades iron oxide nanoparticles have attracted significant investment to develop techniques for tailoring their desirable features, controlling their surface chemistry and developing advanced characterization techniques. A subcategory of iron oxide nanoparticles is superparamagnetic iron oxide nanoparticles.

Superparamagnetic particles exhibit superparamagnetism property which means that they have no permanent magnetic moment. When they are placed in an external magnetic field, they become magnetized up to their saturation magnetization, and in the absence of the magnetic field, they have no magnetic remanence (Fig. 1).[34]

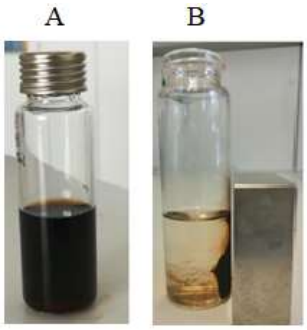

Figure 1: Superparamagnetism property of SPIONs, A)nanoparticles suspension in a vial, B)SPIONs are attracted to a magnet placed closed to the vial producing an external magnetic field, after the removal of the magnet, SPIONs can be dispersed again with no residual magnetic property.

Superparamagnetic iron oxide nanoparticles (SPIONs) are synthetic nanoscale particles of γ-Fe_2O_3 (maghemite), Fe_3O_4 (magnetite) or α-Fe_2O_3 (hematite).[30, 35] Crystal structure of these iron oxides are depicted in Figure 2.

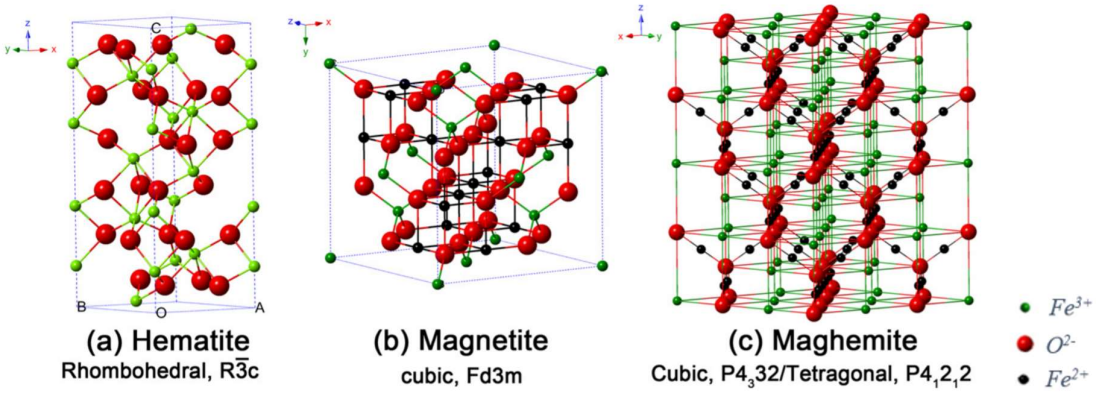

Figure 2: Crystal structure of a) hematite(α-Fe2O3), b) Magnetite (Fe3O4) and c) maghemite (γ-Fe2O3).[25]

For biomedical applications superparamagnetic magnetite and maghemite nanoparticles are the most widely used.[30, 35] The maghemite structure has a cubic symmetry. It is similar to magnetite, but vacancies in the cationic sublattice reduce its symmetry. Each unit of maghemite contains 32 O^{2-} ions, 21⅓ Fe^{3+} ions and 2⅓ vacancies. Maghemite can be considered as fully oxidized magnetite.[25, 36]

Generally, particles in nano-meter size have different electrical, optical, magnetic and chemical characteristics from their atom or bulk forms. Size is a governing factor in environmental fate, behavior, and bioavailability of iron oxide nanoparticles.[37] In biological media, the size and shape influence the pharmacokinetics and biodistribution of NPs as well as the process of recognition and removal by the immune system. NP size can strongly influence the saturation magnetization and the response to external magnetic fields.[38] Superparamagnetic iron oxide nanoparticles applied in biomedicine are generally classified by their hydrated size (including their coating) as oral SPIO at 300 nm- 3.5 um; standard SPIO (SSPIO) at 50- 150 nm; and ultrasmall SPIO (USPIO) at < 50 nm. The iron oxide core size of SPIONs must, however, be smaller than 100 nm in diameter, because superparamagnetism is only observed in particles with a diameter smaller than 20 nm.[34, 35, 39] In a magnetic material, there are regions with all atoms magnetic moments or spins aligned in one direction, called magnetic domain. Inside a bulk magnetic material, there are numerous magnetic domains which are energetically not favored to align parallel to each other or to an externally applied magnetic field. Consequently, these multiple domains interfere with one another and reduce net magnetization. Its size directly influences the number of magnetic domains in each magnetic substance; hence when the particle size is

smaller, specifically in the low nanoscale, the substance becomes a single domain. This means that in the presence of a magnetic field, all domains point in the same direction. Therefore, superparamagnetic nanoparticles possess high magnetic susceptibility and provide a stronger and faster magnetic response compared with bulk magnets. In the absence of a magnetic field, their magnetic domains return to their randomly spin direction and there will be almost negligible magnetic residual. Without a magnetic field, individual magnetic moments are randomly oriented by Brownian motions.[30, 34, 40] Figure 3 shows a simple schematic illustration of the magnetic behaviour of superparamagnetic nanoparticles.

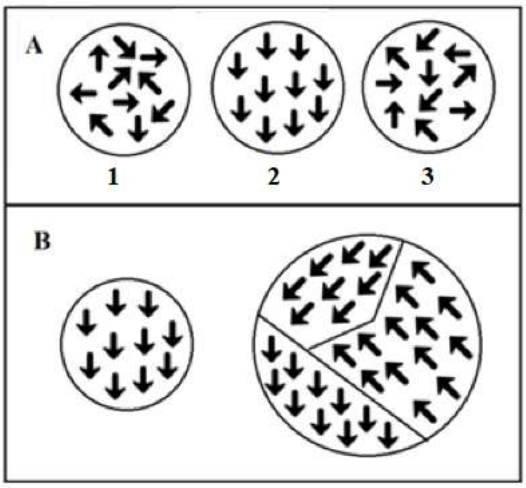

Figure 3: A) Magnetization behavior of SPIONs in the presence and absence of an external magnetic field. 1) SPION crystal in the absence of an external magnetic field, the orientation of the magnetic domains is random. 2) In the presence of an external magnetic field the magnetic moment of SPIONs aligns in the direction of the magnetic field. 3) After the removal of the magnetic field magnetic moments of SPIONs become randomly oriented by thermal excitation. B) Schematic illustration of an ultra-small superparamagnetic iron oxide nanoparticle with a single magnetic domain (all magnetic moments aligned in the direction of the magnetic field) vs. a larger iron oxide particle with multiple magnetic domains, which results in a reduced net magnetization because the domains will interfere with each other.

SPIONs are used in various medical applications[23, 27, 28, 41, 42], production of nanobiocomposites and nanostructures for oil spill and organic contaminants remediation.[43, 44]) The cytotoxicity of superparamagnetic iron oxide nanoparticles has been tested and they have been approved for many biomedical applications.[45] The toxicity of iron oxide nanoparticles is mainly related to particles with no protecting layer or naked particles, since they cause oxidative stress by forming reactive oxygen species.[46] Therefore, the surface of the particles should be passivated by a protecting layer (usually an organic shell, like dextran or polyethylene glycol), which decreases unwanted interactions of particles with the surrounding environment to prevent oxidative shock. As a result of some

synthetic methods, iron oxide nanoparticles are coated with oleic acid, which is their initial covering ligand, placing on particles during the synthesis procedure. Oleic acid-coated nanoparticles completely disperse in nonpolar solvents such as hexane, toluene, dichloromethane and chloroform, and aggregate in polar solvents. For biomedical applications, nanoparticles must be individually sterically stabilized with a neutral organic ligand capable of repelling protein adsorption and thereby fast recognition by the immune system and short circulation time. If the free energy of chain-solvent mixing is negative, strongly solvated ligands will repel each other, which penalizes the overlap of ligands and keep the particles stabilized. On the contrary, if the free energy of chain-solvent mixing is positive, the contact of ligands with surrounding media will be minimized, which will finally lead to the contraction of ligands and aggregation of particles. In physiological media, a dense shell of irreversibly bound ligands with a net neutral charge is needed to achieve particles with high colloidal stability. A bulky neutral organic shell or a short zwitterion shell on the particles have been shown to provide a protective shield for the particles.[47-49]

2. State of Knowledge

2.1 Synthesis of SPIONs

Synthesis of SPIONs has attracted extensive attention in interdisciplinary research because of their scientific and technological importance. SPIONs have been synthesised through different methods including coprecipitation, thermal decomposition, microemulsion and solvothermal synthesis. Common drawbacks of several methods are extensive agglomeration and poor control over size distribution, leading to polydispersity and poor crystallinity of the produced particles; therefore, an additional size sorting step is encouraged for these method.[50, 51] Among the synthesis methods, thermal decomposition stands out for providing precise control over the size distribution, shape, and crystallinity.[50] Generally, in thermal decomposition methods an iron-containing precursor decomposes at high temperature to form iron oxide nanoparticles. The precursor is injected into a solvent in presence of a capping agent. Frequently used precursors in these methods are iron (III) oleate ($Fe[C_{18}H_{33}O_2]_3$), iron oxyhydroxide (FeOOH) or iron pentacarbonyl ($Fe[CO]_5$).[52] Reaction conditions such as the precursor to capping agent molar ratio, temperature, heating ramp and time control size and size distribution of the synthesised nanoparticles. SPION synthesis via hot-injection and heat-up methods falls under the thermal decomposition category.

The heat-up synthesis method for SPIONs between 4-16 nm was reported by Hyeon et al. in 2001.[53] In the heat-up method, the iron precursor is iron pentacarbonyl, which decomposes at a temperature between 260-320 °C in dioctyl ether as a nonpolar solvent in the presence of oleic acid as a surfactant. The resulting size distribution by this method is quite narrow ($\sigma \leq 5\%$), but the size range that can be synthesized is limited. For manufacturing SPIONs with a larger size, a hot-injection procedure must be adopted.

The hot-injection method was also introduced by Hyeon et al. In this method, iron oleate ($Fe(OA)_3$) is used as the iron precursor and injected rapidly into a solution containing a solvent and a capping agent.[54] The reaction temperature is around 300°C and will drop after a certain time. Nuclei formation burst after hot injection because of a high supersaturation level. However, temperature drop leads to preventing of further nuclei formation and growth of already formed nuclei and narrow size distribution ($\sigma \leq$ 8-14%) of synthesised particles.[55] The developed thermal decomposition synthesis methods produce γ-Fe_2O_3 nanocrystallites and offer several advantages such as reproducibility, scalability, high yield, delivering highly crystalline and monodisperse nanoparticles without laborious

size sorting process, tuneable size and size distribution by changing the reaction parameters such as reaction time, temperature, concentration and ratios of the reactants, solvent, precursors, and addition of seeds. Additionally, the nanoparticles can be dispersed without aggregation in many hydrocarbons. However, the disadvantage of this method is that the produced nanoparticles have a dense shell of oleic acid, which is a hydrophobic ligand and not suitable for application in biological media.[41, 53] Therefore, these SPIONs should be stored in nonpolar solvents like hexane. For biomedical applications, these particles require post-synthesis surface modification.

2.2 Surface modification and functionalization of SPIONs

Although dimensions of nanoparticles make them ideal for the production of nanostructures for many biotechnological applications, further surface modification of these nanoparticles is essential. In order to understand the surface modification process, a brief introduction about the core-shell nanoparticle structure is required. Simple nanoparticles are composed of a single material, but core-shell nanoparticles are made from two or more materials, an inner material or core and an outer layer material or shell (Figure 4). The covering shell can be various types of organic and inorganic compounds, depending on the end application and desired features.[56]

Figure 4: Simple graphic of a concentric spherical core-shell nanoparticle, consisting of a simple inner core and a shell of a different material.

Functional properties of these nanoparticles are strongly affected by the ligand shell, which are covering the cores, determining surface and colloidal characteristics and hence, stabilizing and preventing nanoparticles from aggregation in applications such as composite or medical materials. Therefore, both the size and the shell of organic ligands play crucial roles in nanoparticle application.[22, 29, 41, 56]

In physiological media, a shell of polymers or ligands must cover SPIONs to have dispersed nanoparticles and avoid interactions between particles themselves and with aqueous media, which lead to aggregation and precipitation out of solution. The stabilizing ligands of the shell are often called dispersants and multiple types of dispersants can compose the shell. Figure 5 is a schematic representation of the type of core-shell SPION investigated in this thesis and its details will be discussed in the following sections.

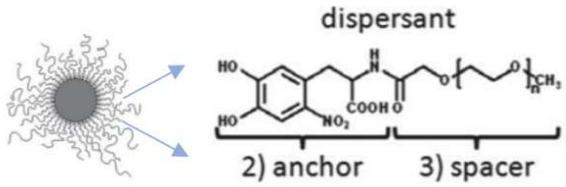

Figure 5: Scheme of core-shell nanoparticle with a magnification of the structure of dispersant ligand including nitrodopamine ancho and PEG spacer[57]

2.2.1 Polyethylene glycol as shell dispersant and its competitors

In recent years, several natural and synthetic polymer ligands, such as dextran [42, 57], starch[58], polyethylene glycol (PEG)[20, 59-61] have been used to coat different forms of SPIONs to make them dispersable in physiological media. However, PEG and dextran are the most extensively used polymer ligands, because they are biocompatible and classified as Generally Regarded As Safe (GRAS) substances by FDA, and also because they are not very rapidly recognized by body immune system and macrophages in liver and spleen in intravenous administration.[62, 63] High biocompatibility of PEG $(C_2H_4O)_n$ and PEGylated coatings make them ideal for increasing blood circulation time of nanoparticles. Molecular weight and surface density or grafting density of PEG coatings are two main factors that influence the stability, cytotoxicity and vascular circulation time of nanoparticle dispersions.[58, 64] Dextran $(C_6H_{10}O_5)_n$ and its derivatives are applied as a covering agent in some commercially available superparamagnetic iron oxide nanoparticles. Dextran is highly biocompatible and has no direct cytotoxic effects, but the common dextran shells have some drawbacks. The dextran coatings degradation may influence certain cellular processes.[27, 65] Furthermore, molecular weights of dextran coatings are higher than 10 kDa; they have poor binding affinity towards iron oxide and therefore demonstrate reversible adsorption to the surfaces of nanoparticles. Consequently, dextran shell often enwrap multiple iron oxide nanoparticle cores by direct physisorption to nanoparticle surfaces.

Therefore, multiple iron oxide nanoparticle cores are encompassed in one cluster and obviously the cluster hydrodynamic diameter is many times larger than the single nanoparticle core diameter. However, it is not easy to control the cluster size. In contrast, low molecular weight dispersants like PEG can embed single cores of superparamagnetic iron oxide nanoparticles and provide tunable hydrodynamic size. Hence, stabilization of superparamagnetic iron oxide nanoparticles with low molecular weight (<10 kDa) dispersant ligands like PEG(5 kDa) result in explicit core-shell nanoparticles composed of four components: core, anchors, spacers and optionally functionalities. These dispersants consist of a polymer spacer with a covalently bound anchor that has a high affinity for the nanoparticle surface [66], such as PEG bearing a nitrodopamine anchor (Figure 5). PEG is a hydrophilic, water-soluble, biocompatible polymer. The use of PEG to increase the biocompatibility of iron oxide dispersions and blood circulation times have been reported in several researches. The PEG-coated nanoparticles revealed excellent solubility and stability in aqueous solution as well as in physiological saline.[41, 67]

A major challenge has been to achieve a dense grafting of dispersants also onto monodisperse cores since such cores are already coated with a high-affinity capping of oleic acid after synthesis. Oleic acid is difficult to replace with another dispersant at high density. PEG is widely used in providing nanoparticles with stealthy properties. A thicker and denser shell has been shown to result in higher colloidal stability under challenging environmental conditions, including high concentrations of biomolecules [68]. It was reported that a grafting density of 1 PEG/nm^2 on spherical gold nanoparticles with a size of 50 nm, showed less protein adsorption and cell uptake and subsequently longer blood clearance time in comparison with grafting density of 0.5 PEG/nm^2[69].

2.2.2 Nitrodopamine anchor

The dispersant shell must be attached firmly to nanoparticle surfaces through suitable anchors. Particular attention must be given to the selection of anchors because of their importance for the surface modification and stability of sterically stabilized nanoparticles.[66] The best anchors have high binding affinity and low desorption rate k_{off} so that they can irreversibly bind spacers to uncoated nanoparticles and are able to replace hydrophobic capping agents such as oleic acid often used to synthesize monodisperse

superparamagnetic iron oxide nanoparticles. Catechol derived anchors like nitrocatechols are common anchors used in surface modification of superparamagnetic iron oxide nanoparticles.[70] Catechol derivative anchors combine high binding affinity to iron oxide nanoparticles surfaces and low desorption rates if properly modified. To optimize the affinity of this type of anchor to iron ions in Fe_3O_4, they are electronegatively substituted. The strong complexation of nitrocatechols to Fe^{3+} ions and increased electron density at the nitrocatechol anchors result in high stability of grafted polymer films when nitrocatechols are used as anchors. SPIONs with shells of PEG-nitroDOPA or PEG-nitrodopamine were much more stable than iron oxide NPs stabilized with PEG-DOPA and PEG-dopamine. Furthermore, nitroDOPA and nitrodopamine indicated essentially irreversible binding to iron oxide nanoparticles under physiologic conditions, in stark contrast to other investigated catechol-derivative anchor groups.[66, 70, 71]

2.3 Ligand replacement approaches

2.3.1 Grafting to/ Grafting from

There are two major routes to place a polymer ligand on a nanoparticle core; “grafting from” and “grafting to” (Figure 6). In the “grafting from” technique, a small molecule initiator such as nitrodopamine covalently binds to nanoparticle surface and replaces the covering agent like oleic acid. In the second step, a spacer polymer grows and polymerizes from the nanoparticle surface on the initiator, which is already attached to the surface of the nanoparticle.[68] Drawbacks of this method include poor control over ligand polymerization, which leads to nonuniform and polydisperse polymers, inhomogeneous dispersant layer thickness or poorly dispersible particles. Additionally, this approach requires oxygen-free conditions for most common polymerization techniques and very careful removal of excess unattached initiator prior to polymerization in order to avoid unwanted termination of the polymerization or polymerization in solution.[50]

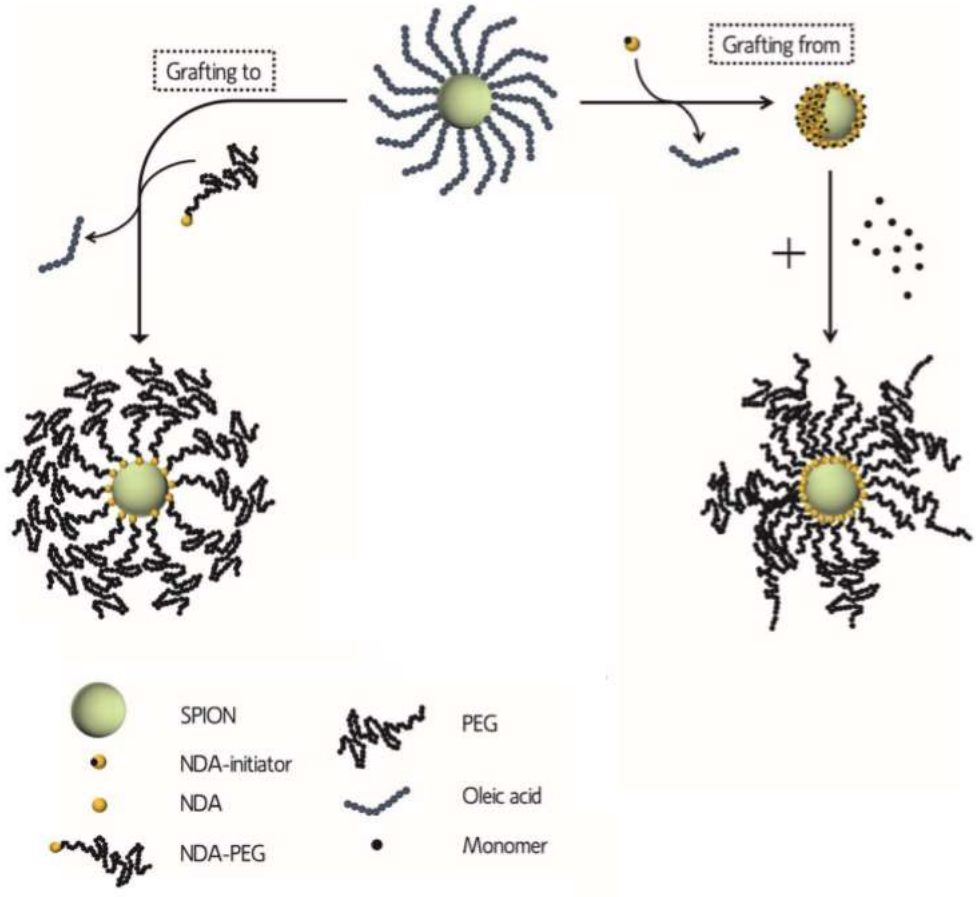

Figure 6: Two main ligand exchange methods; in "grafting to" the complete polymer ligand including the anchor and spacer is synthesized separately before the ligand exchange. During the regrafting these pre-made ligands replace the initial covering agent due to higher affinity. The "Grafting from" approach is a two-step process in which an initiator is attached to the NP surface and replaces the capping agent during the first step. In a second step, an in situ polymerization of the polymer ligand happens and the dispersant regrafting is completed.[50]

In the "grafting to" approach, the ligands are synthesized separately before the main ligand grafting stage. Afterward, as shown in Figure 6, the synthesized dispersant is grafted to the surface of nanoparticles due to higher affinity to iron oxide nanoparticle surface, for example, PEG polymer ligands bearing nitrodopamine replace the initial oleic acid capping agent which has a lower affinity to the nanoparticle surface. This process can be done in one step or a two-step protocol. This method is applicable for a wide range of polymer ligands; therefore, according to the desired application, the nanoparticle structure can be tailored, and this is the main advantage of the "grafting to" method. Furthermore, this approach is reproducible and saleable. This method has two drawbacks. The first one is the low grafting density of the ligand shell because of the repulsion of adjacent ligand molecules and steric hindrance, which leads to fewer molecules being attached to the nanoparticles surface and

decrease grafting density. Second, traces of the initial capping, e.g., oleic acid that remain bound to the nanoparticle surface and might be an issue in specific applications.[47, 66]

2.3.2 Direct ligand exchange/stripping-regrafting

In this work, two strategies were adopted to replace oleic acid shell with a suitable organic ligand, both pursuing a grating-to approach rather than grafting-from. The first strategy is a melt ligand exchange or direct ligand exchange, where the hydrophobic ligands on the SPIONs are replaced by ligands with higher affinity such as nitrocatechol containing ligand (Figure 7A). In this method, the ligand replacement is fulfilled in one step in which the polymer ligand itself is the solvent, and thus, its effective coil size is minimal to ensure a small grafting footprint and increase grafting density on the nanoparticle surface. However, the final particles may contain residuals of the initial ligand (oleic acid) in the shell.[72]

The second technique is a recently developed method, consisted of stripping the nanoparticle surface from the original covering agent and then regrafting of certain ligands on the surface of naked nanoparticles.[47] For end-applications in which complete removal of oleic acid from the nanoparticle surface and replacement of a hydrophilic ligand is of vital importance, a two-step approach of stripping and regrafting with the ligand of interest could achieve optimal results (Figure 7B).

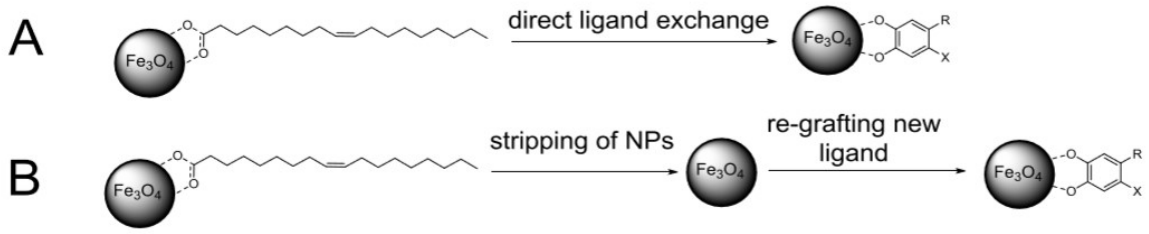

Figure 7: Nanoparticles surface modification strategies: a) direct ligand exchange, b) stripping-regrafting, A) direct ligand exchange, B) stripping-regrafting[68]

The stripping/regrafting method is a two-step procedure. During the first step, the capping agent is removed and nanoparticles become stripped from their original shell. In a second step, the desired ligand is regrafted on the nanoparticle surface (Figure 7B). Hence, a specific stripping agent is required to change the equilibrium of the binding of the original ligand on the nanoparticle surface to strip the particles. The stripping agent should have a sufficiently low affinity to the nanoparticle surface to be efficiently replaced by the ligand of choice with

a higher affinity to the nanoparticle surface. In our approach, this completely removes the oleic acid from the surface of SPION using crown ether and sodium or potassium halide salts as the stripping agent (Figure 8). Crown ether complexes the cation, i.e., Na^+ or K^+. The formation of the crown ether-cation complexes frees the halide anions and changes the equilibrium of the halide; it shifts the binding equilibrium at the SPION surface such that the abundant halide displaces oleic acid because of its also significant affinity for the iron oxide surface. Since pristine oleic acid-coated nanoparticles are dispersible in nonpolar solvent, the stripping step takes place in a nonpolar solvent like hexane. Thereafter, nanoparticles are transferred to a polar solvent like DMF because the hydrophobic shell is detached, and iron oxide nanoparticles are not hydrophobic anymore. Removed oleic acid molecules remain in nonpolar solvent and leave the reaction solution. The resulting particles can be completely oleic acid-free. The naked particles can be regrafted with an organic shell.[72]

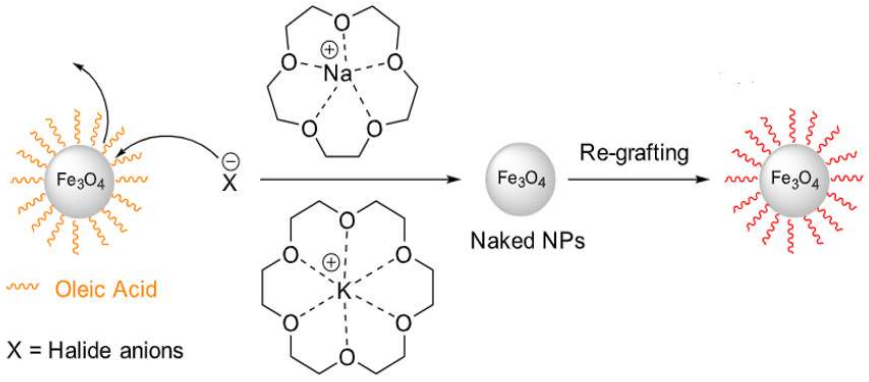

Figure 8: Stripping of nanoparticles and grafting of different ligands on naked nanoparticle surface using halide exchange and crown ether complexation. Crown ether such as 18-crown-6 and 15-crown-5 complex the potassium or sodium cations from halide containing Na and K salts such as KF, NaF which leads to their dissociation and producing halide anions. These halide anions have higher affinity to iron oxide surface than the original oleic acid capping agent and can easily displace OA from NP surface. The crown ether-cation complex is further washed out from the reaction solution.[72]

This method is reproducible, non-costly and easy to handle, highly efficient and free of remaining the original oleic acid capping agent. Some hydrophobic ligands have been previously successfully regrafted on SPIONs and in this work regrafting a dense hydrophilic ligand shell was investigated.[47, 72]

2.4 Purification

The last and most important step of surface modification is removing the excess unbound dispersant molecules from the solution to keep the firmly adhered ligands and validate the outcome using state-of-the-art characterization techniques. The complete expelling of free, unattached ligands and residuals of original capping agent from the reaction solution has always been a crucial and challenging stage of nanoparticle synthesis. The presence of remaining free ligands results in the overestimation of the grafting density on the nanoparticle surface. Hence, achieving nanoparticle samples clear of all sorts of impurities is very important for both characterization and end-application. However, intensive purifying can lead to particle degradation, aggregation and precipitation.[66, 73] Basically, purification methods are based on the properties of core or anchor of unbound polymer ligand. As an example, magnetic separation purification is based on the magnetic moment of the core-shell nanoparticles. Purification on the grounds of the anchor group affinity or solubility is used in many purification techniques. Affinity purification methods use either electrostatic or complexing interactions between the unattached anchor group (nitrodopamine) and a surface to separate nanoparticles from unattached excess ligand on a column or via spinning down and precipitation from a denser colloidal material with an affinity for the anchor group. Solubility-based purification methods reduce the solubility of the nanoparticle shell as well as of the free ligand. The particles can be aggregated faster than free polymer ligand due to the high polymer density in their shell and the van der Waals attractions of the cores which then facilitates magnetic extraction of magnetic nanoparticles so that it can be achieved with moderate magnetic field strengths. Reducing the solubility can be achieved by reducing the solvent quality of the nanoparticles. Moreover, size exclusion methods sort out the unattached ligands from the grafted nanoparticles according their size.[66, 73, 74] Important is that the purification method can be scaled to large batch sizes and remains economically viable.

2.5 SPIONs as contrast agents

Magnetic Resonance Imaging (MRI) is a non-invasive medical imaging technique that derives directly from the phenomenon of Nuclear Magnetic Resonance (NMR). It is widely used to determine molecular structure. The principle of NMR is based on that an unequal

number of protons and neutrons in the nuclei of atoms leads to their interaction with an external magnetic field through a non-zero net spin. Since there is a huge amount of water molecules inside the human body, MRI focuses on measuring hydrogen in water molecules, coined the "^{1}H proton" to generate the signal. The signal intensity is proportional to the quantity of ^{1}H protons and therefore the amount of H_2O in the tissue. In NMR/MRI, the energy difference between the excited state and steady (equilibrium) state is too low to allow spontaneous relaxation, and therefore relaxation needs to be stimulated.[45, 50, 75, 76] Using contrast agents is not a compulsory prerequisite for MRI experiment, and it is not the contrast agent itself that is visible. In fact, the MRI contrast agents increase image contrast and diagnosis accuracy through interaction with ^{1}H protons of tissue cells,[77-80] and either modify their relaxation times or directly get involved in the level of ^{1}H proton magnetization. Therefore, signal differences in adjacent tissues due to different proton densities result in contrast enhancement. MRI applications are becoming more and more dependent on contrast agents. The combination of MRI and contrast agents greatly enhances the possibilities to depict the vascular system, inflamed tissue as in arthritis, tumour angiogenesis, atherosclerotic plaques and the breakdown of the blood–brain barrier related to pathologies such as multiple sclerosis. Within the emerging field of cellular and molecular MRI, contrast agents have become an essential element of the technique.[45, 81]

Contrast agents are classified as paramagnetic metal ion-ligand complexes and superparamagnetic particles. Gadolinium ion (Gd^{3+}) containing compounds are main paramagnetic contrast agents.[45] Free gadolinium is toxic to humans and must be bound to a chelate or ligand. For many years it was believed that gadolinium-based contrast agents were safe, which led to the free use of these agents. However, time has shown that Gd-based contrast agents are not inert. The major deficiency caused by theses contrasting agents has been reported to be their causative role in nephrogenic systemic fibrosis (NSF), an almost new and serious disease that might lead to death or serious damages to patients with early-stage renal disease (ESRD). Gadolinium deposition within human bone, neural and brain tissue is considered as another adverse effect of Gd-containing contrast agents.[77-80] Adverse reactions to Gd-based contrast agents are more common in patients with a history of asthma, allergies, renal insufficiency, and in patients injected at a faster rate.[82, 83] Due to these drawbacks of Gd-based contrast agents, developing a promising alternative, especially for patients with kidney diseases, is gaining more attention.

Although iron-based contrast agents have been around for many years, they did not generate substantial clinical interest until the emergence of safety concerns regarding Gd-based contrast agents. Iron-oxide contrast agents, such as superparamagnetic iron oxide and ultrasmall superparamagnetic iron oxide nanoparticles, have been investigated for MRI for more than two decades. These particles perform like small transferable magnets and generate a strong magnetic field heterogeneity in the surrounding area and significantly reduce the relaxation time of water protons (^{1}H) in their vicinity. SPIONs can be employed in medical fields for magnetic resonance imaging (MRI), magnetic particle imaging (MPI), targeted delivery of drugs, proteins, antibodies, and nucleic acids, hyperthermia, biosensing, tissue repair , and separation of biomolecules.[22, 27, 42, 45, 77]

Most important properties of SPIONs include their capability to exhibit magnetization only in the presence of an applied external magnetic field; their ability to form stable colloidal suspensions which is crucial for biomedical applications, faster relaxation, capability of control over their composition, size, shape, and surface chemistry make them a potential alternative to current Gd-CA. Several iron-oxide nanoparticles have been clinically tested, and a few have been approved for clinical use in certain countries, at least for a short period. For example, Feridex I.V., Resovist and GastroMARK; although their production was discontinued and they were withdrawn from the market mainly baecause of poor sales in 2008, 2009 and 2012 respectively. Ferumoxytol, a Food and Drug Administration (FDA)-approved intravenous medication for treating iron-deficiency anemia, was shown to be an excellent contrast agent for MRI in patients with severe kidney disease who should not get Gd-based contrast agents due to NSF risk.[28, 84, 85] Additionally, as a result of the growth of higher magnetic field MRI scanners in clinical practice, iron oxide-based contrast agents have gained increased importance due to differences in their functioning mechanism they accomplish better results in higher field strengths.[45, 50, 86]

In medical applications of SPIONs, control over monodispersity and size is very important because the properties of the nanocrystals significantly depend on the dimensions of the nanoparticles. In summation, for biomedical applications nanoparticles require high magnetization values, smaller than 100 nm size, narrow particle size distribution and also biocompatible and nontoxic surface covring shell. It should preferably also allow for targeted delivery, which means localizing the particle in a specific tissue. Magnetic nanoparticles can attach to proteins, drugs, enzymes and antibodies or can be guided to an organ, tissue, or tumour with applying an external magnetic field.[41]

2.6 Biodistribution and fate of SPIONs inside body

The biodistribution of SPIONs is highly dependent on the administration route, thickness and type of coating ligand, size and surface charge of the particles. Under normal circumstances, intravenously injected SPIONs with a hydrodynamic size of about 100 nm are sequestered by the immune system, bone marrow and/or spleen, and thereafter metabolized and regulated by normal physiological iron homeostatic mechanisms. SPIONs are cleared from the blood circulation following intravenous administration by the mononuclear phagocyte system, with almost 80% being removed by the liver Kupffer cells. Following intravascular injection, the nanoparticles are removed within 3-7 weeks, with the highest spike in liver uptake occurring in the first 6 hours. SPIONs have relatively long blood circulation time and this allows for imaging to be performed hours or even days after injection. Regardless of the vascular circulation time, after SPIONs intracellular uptake, lysosomes metabolize SPIONs into a soluble and nonsuperparamagnetic form of iron. This iron compounds are then taken up into the normal iron metabolism pathways of the body and used in the production of iron-containing proteins such as hemoglobin and transferrin and therefore become part of the normal iron pool. Although, increased blood serum iron levels can induce mild oxidative stress, but this happens only with administration of repeated or high doses; no direct links to chronic or acute adverse effects were indicated. The most frequently reported negative events of SPIONs are back pain in 4% and flushing in 2% of the target population. In addition, there are concerns about anaphylactic reactions which limit SPIONs use in the clinic.[22, 28, 87, 88]

2.7 Scope of the thesis

Monodisperse superparamagnetic iron oxide nanoparticles are synthesized using thermal decomposition of, e.g., Fe(CO)5 precursors in the presence of oleic acid. This leaves nanoparticles with a hydrophobic shell of oleate and decomposition products thereof that are difficult to displace. For application in medicine and biotechnology, the nanoparticles have to be surrounded by a hydrophilic shell that prevents attractive interactions with proteins and other biological molecules. The common and preferred solution to this is grafting of a dense shell of hydrophilic polymer. In medical applications the preferred polymer to date is poly(ethylene glycol) (PEG), which must be densely grafted to the nanoparticle surface. The

following problems are difficult to solve for the synthesis of monodisperse SPIONs grafted by a sufficiently dense PEG shell for medical and biotechnological applications:

1. Displacement of the oleate shell
2. Dense grafting of a hydrophilic polymer. The grafting density should ideally be >1 chain/nm^2 of hydrophilic polymers with a degree of polymerization >100.
3. Purification of excess polymer ligand from the nanoparticles
4. Reuse of excess polymer ligands

So far, suitable solutions in the best case exist only for the lab-scale synthesis of hydrophilic, polymer-grafted superparamagnetic iron oxide nanoparticles. In this thesis, I investigate ligand stripping, replacement, and purification methods that could improve on these limitations.

Point one might not be required for the colloidal stability of the nanoparticles if point two is still realized. However, point 1 is believed to greatly enhance the relaxivity, in particular the T1 relaxivity, of the particles, since a larger volume of water in direct proximity of the magnetic particle surface increases the relaxivity. This is a decisive measure of the quality of such nanoparticles as contrast agents, which is their current main application.

The theoretical maximum grafting density on iron oxide nanoparticles is believed to be ~3 chains/nm^2 (dependent on the assumptions made for the limiting factor of the density of high-affinity grafting sites).

Point 3 is crucial to correctly estimate the colloidal stability of the particles and to avoid undesired side effects of free ligands during experiments and applications. It was until recently often neglected in the literature but has increasingly come into focus as the reliability of many findings where the purity of the samples was not ensured has been questioned. Finding a solution that, with minimum effort, cost and time, ensures purification of the nanoparticles in large amounts (batches or preferably continuously) is, therefore, key to continued development. Today the main method is dialysis from several days to a week since the physicochemical properties of the polymer-grafted nanoparticles and free polymers are very similar.

Choosing a clever purification method that makes it possible to recapture the large amount of excess polymer ligand that must be used during efficient grafting would greatly reduce the costs of nanoparticle synthesis, hence point 4.

Therefore, the goal of this thesis is to develop monodisperse and colloidally stable core-shell superparamagnetic iron oxide nanoparticles with a dense shell of biocompatible ligand for application in biomedicine as a contrast agent that fulfils or improves on the listed 4 points compared to the current state-of-the-art.

3. Materials and Methods

3.1 Material

Iron(0)pentacarbonyl (99,99% trace metal basis), oleic acid (≥93% technical grade), dioctyl ether (>99%), dopamine hydrochloride (≥98%), sulfuric acid (95-98%), sodium nitrite (≥99%), 4-Methyl-morpholine (99% ReagentPlus), (1-Cyano-2-ethoxy-2-oxoethylidenaminooxy)- dimethylamino-morpholino-carbenium hexafluorophosphate (COMU, 97%), hydrochloric acid (37% ACS reagent), Sephadex G75 (superfine), bovine calf serum (sterile filtered, for cell culture) and phosphate buffered saline (PBS 10x concentrate BioPerformance certified) were purchased from Sigma Aldrich, Methoxy-PEG acetic acid (MeO-PEG-COOH, Mw 5000) from JenKem Technology, EtOH (>96% technical grade), DMF (>99,9% ACS reagent), CHCl3 (≥99.5% containing 100-200ppm amylenes as stabilizer), n-hexane (≥95% chromasolv plus for HPLC) and petroleum ether (30-50°C bp, p.a.) were obtained from Carl Roth. Bovine serum albumin (BSA) was purchased from Bio-Rad. Ultrapure Milli-Q water (Millipore USA, R=18MΩcm) was used for all experiments. 1000kD MWCO Float-ALyzer regenerated cellulose dialysis membranes were purchased from Spectrum Labs Netherlands. All chemicals were used as received without further purification.

3.2 Synthesis of SPIONs

For the synthesis of iron oxide nanoparticles, two thermal decomposition methods were used, depending on the targeted nanoparticle size.

3.2.1 Heat-up method

Small SPIONs (4-16 nm in diameter) stabilized with oleic acid (OA) were synthesized by a slightly modified version of heat-up method according to a method reported by Hyeon et al.[53] Briefly, Oleic acid-coated superparamagnetic iron oxide nanoparticles (OA-SPIONs) were synthesized via thermal decomposition of iron(0)pentacarbonyl. In a typical procedure, a solution of 50 mL dioctyl ether (Oct_2O) containing respective amount of oleic acid (molar ratio of $Fe(CO)_5$:OA for smaller NPs 1:2, for larger NPs 1:3) was heated to 100 °C with a ramp of 10 K/min under constant flow of N_2 and was kept in this temperature for 10 min to

remove any traces of H_2O. Afterward, 1 mL of iron(0)pentacarbonyl was injected rapidly into the solution. The temperature was then gradually raised to reflux with a ramp of 3 K/min and held at 290 °C for 1 h. The synthesized iron oxide NPs were subsequently cooled to room temperature, precipitated with EtOH and collected with an external magnet. The particles were washed 5 times with ethanol and centrifuged at 5000 rpm for 1 minute to remove the excess of oleic acid and dioctyl ether.[50] In this method size of SPIONs could be adjusted by changing reactants ratio and reaction temperature, as an example, for 10.4 nm SPION, amount of oleic acid was 7.0 mL.

3.2.2 Hot-injection method

Large particles (>11-22 nm) were synthesized according to a hot-injection method reported by Park et al.[54] In this method iron oleate complex (Fe-OA) was synthesized by mixing 3.6 g of $FeCl_3 \cdot 6\ H_2O$ and 12.17 g of sodium oleate in 26.7 mL of EtOH, 20 mL of Milli-Q, and 46.6 mL of n-hexane. The mixture was refluxed at 70 °C for 4 h and allowed to cool to room temperature. After washing the organic layer thrice with 30 mL of Milli-Q, the solvent was removed and the Fe-oleate complex was obtained as reddish viscous material in 98% yield. In a second step, SPIONs were synthesized as follows: 6.6 g of Fe-oleate complex was mixed with 0.56 mL of OA and 25 mL of (Oct_2O). The mixture was heated to 100 °C under a constant flow of N_2 to remove traces of water. After heating to 290 °C with a temperature ramp of 3 °C/min, the mixture was aged for 90 min and cooled to room temperature. SPION size was controlled by the Fe-oleate:OA ratio.

3.3 Synthesis of 6-nitrodopamine-hemisulfate

NDA-HSO_4 was synthesized using according to the literature with slight modifications.[89] 2.5g dopamine hydrochloride (DA-HCl 26.36 mmol) and 6.3g sodium nitrite ($NaNO_2$ 81.17 mmol) were dissolved in 150 mL deionized water and cooled in an ice/NaCl bath. 25 mL of 20% sulfuric acid were added dropwise under vigorous stirring to the cooled solution maintaining the temperature below 10°C. After complete addition, the reaction mixture was slowly warmed to room temperature and reacted overnight. The resulting yellow precipitate

was collected by filtration and washed excessively with ice-cold water and once with MeOH. NDA-HSO_4 was obtained as intense yellow powder in 54% yield.

3.4 Synthesis of PEG-nitrodopamine

6-Nitrodopamine-poly(ethylene glycol)(5000) (NDA-PEG(5kDa)) was synthesized via (1-Cyano-2-ethoxy-2-oxoethylidenaminooxy)-dimethylamino-morpholino-carbenium hexafluorophophate (COMU) mediated peptide-coupling reactions.[74, 90] Typically, 5 g MeO-PEG(5000)-COOH were dissolved in 30 mL DMF and pre-activated for 30 min at room temperature with 0.64 g COMU. The mixture was purged with N_2 for 20 min and cooled to 4°C. 0.24 g of NDA-HSO_4 were dissolved in 2 mL DMF and mixed with 257 µL n-methylmorpholine (nMM). After 10 min the amine-containing solution was added dropwise to the activated PEG at 4°C under N_2. The solution was slowly warmed to RT and reacted for 48h. 90mL 3M HCl were added to the mixture and extracted 3x with $CHCl_3$. The solvent was removed under reduced pressure and the product was collected as a light-yellow powder in 65% yield verified by ^{1}H-NMR.

3.5 Polymer ligand grafting on SPIONs

3.5.1 NPs functionalization via stripping-regrafting

A previously developed stripping-regrafting for organic ligands on iron oxide nanoparticles[72] was adapted by adding a step of melting. In brief, N_2 dried OA-NPs (50 mg) were dispersed in hexane (50 mL), isopropanol (40 mL) and KF-18-crown-6 complex (50 mg in 3 mL water) were added. Naked NPs precipitate immediately by gentle shaking of the NP dispersion, this can be subsequently followed by a centrifugation step to spun down the NPs but this centrifugation requires after the addition of isopropanol to decrease the surface tension of the solvent interface. Precipitated SPIONs were washed several times with hexane, isopropanol and water, respectively, to remove residual oleic acid, salt and crown ether. The samples were N_2 dried and weighted and the respective amount of PEG(5 kDa)-nitrodopamine was calculated for each nanoparticle size using grafting density equation (Equation 1) with an excess of 4-8 times as the needed amount of ligand. According

to the original method for regrafting, PEG-NDA was dissolved in dimethylformamide (DMF) and stripped nanoparticles were added and ultrasonicated for 24 h. Here, regrafting of PEG-NDA was slightly modified compared to the previous approach for regrafting of the hydrophobic ligand[72]. In the new approach PEG-NDA was dissolved in DMF and added to the naked SPIONs. The suspension was sonicated for 3h in the presence of DMF to mix ligand and the naked particles evenly. However, due to the low colloidal stability of the naked particles, the regrafting approach was followed by removing the solvent under reduced pressure using Rotavapor at 60 °C. In order to complete removal of solvent, further evaporation was done using a lyophilizer (RT, 0.05 mbar) for at least 48 hours. In order to efficiently disperse ligand and naked particles, the dried film (naked SPIONs and ligand) were heated for 90 min at 110 °C. Solvent-free conditions and elevated temperature help the ligand to reduce its size and make it small enough to intercalate between the already attached ligands on the surface of the SPIONs, which leads to higher grafting density of ligand on the surface of SPIONs.

3.5.2 SPIONs functionalization via direct ligand exchange

Modification of SPIONs through direct ligand exchange was also done by slight modification. Oleate-coated SPIONs (50 mg) were dispersed in dry DMF (5 mL) under inert atmosphere and PEG-(5 kDa)-nitrodopamine was added in respective amounts according to the size of the SPIONs and using Equation 1 to estimate the grafting density, with the use of an excess of 4 times as the amount of ligand needed for successful grafting of a dense shell. The suspension was ultrasonicated for 3 h. The samples were lyophilised for 48h to remove any traces of the solvent after evaporation of DMF in a Rotavapor. Afterward, the sample was heated to a melt of the polymer and kept at 110 °C for 90 min.

3.6 Purification methods

Various approaches were tested to evaluate different purification methods of separating PEGylated particles from free PEG. The products from all purification methods were characterized by TEM, DLS, and TGA.

3.6.1 Membrane dialysis

Before adding the particles, the membranes were activated for 20 min in 10% v/v EtOH and 30 min in H_2O. Lyophilised re-grafted SPIONs were dispersed in 5 mL distilled water and dialyzed for 72 h against 5 L water in 1000 kDa molecular weight cut-off (MWCO) membranes (being refilled twice a day). In order to remove any traces of SPIONs aggregates, the purified suspensions were centrifuged at 5000 rpm for 1 minute, and the supernatant was freeze-dried to obtain the functionalized SPIONs as dark brown solids.

3.6.2 Magnetic decantation

Almost 100 mg of regrafted SPIONs were dissolved in 10 mL of EtOH by sonication and slight heating with a heat gun at 60 °C. The clear dispersion was poured into a small beaker and mixed with 10 mL of ice-cold petrol ether whereupon it got slightly turbid. The beaker was placed on a 5 × 5 cm 1 T magnet in the fridge at 4 °C, and the NPs were soaked from the cloudy mixture to the bottom of the beaker within a few minutes, dependent on the SPIONs size. The supernatant was decanted by holding back the NPs with the magnet. Collected SPIONs were again dissolved in 10 mL of EtOH, dispersed by hot gun and separated by the addition of petrol ether, followed by magnetic decantation. This procedure was repeated seven times; afterward, samples of SPIONs were freeze-dried and obtained as a dark brown powder.

3.6.3 Membrane centrifugation

Crude sample (regrafted) (750 mg) was dispersed in 15 mL of Milli-Q and loaded into a centrifugation filter (1000 kDa Amicon-Ultra15 membrane) and centrifuged at 4500g for 15 min. The centrifuge effluent was collected, and the sample was re-dispersed in 10 mL of Milli-Q to continue centrifugation steps.[74] This procedure was repeated up to 12 times. During the purification process, aliquots of the samples were taken after 5, 7, 10, and 12 centrifugation steps to track the removal of excess NDA-PEG.

3.6.4 Al_2O_3 application

5 mg of the NPs were dispersed in Milli-Q water containing Al_2O_3 (100 mg/3 ml), kept stirring for 2 hours and centrifuged at 5000 rpm for 1 minute, unattached ligands precipitate with the aluminium oxide and the supernatant containing the nanoparticles was extracted. This was repeated 5 times to collect samples and lyophilise them for further experiments.

3.7 Proton nuclear magnetic resonance spectroscopy (^{1}H-NMR)

^{1}H-NMR spectra were recorded on a Bruker Avance III 500 MHz spectrometer at room temperature using D_2O or $CDCl_3$ as solvents. NPs were dissolved in concentrated HCl and the shell material was extracted with chloroform.

3.8 Transmission electron microscopy (TEM) acquisition and image analysis

A small amount of specimen was dispersed in water (PEG-grafted NPs) or toluene (as-synthesized nanoparticles) and dropped onto a TEM-grid (3.05 mm HR-TEM grid, copper 300 mesh, carbon film). TEM images were obtained using FEI Tecnai G2 200 kV transmission electron microscope at 200 kV. Core diameters were estimated by using ImageJ and Pebbles software package with a local intensity fitting algorithm.[91] For this analysis, generally, more than 1000 particles were sampled by Pebbles.

3.9 Thermogravimetry analysis (TGA): Grafting density calculation

Samples of 1−3 mg each were weighed in 70 µL Alumina-cups and measured on a Mettler-Toledo TGA/DSC 1. The samples were measured under a constant flow of synthetic air (80 mL/min) plus 20 mL/min nitrogen stream as protection gas for the balance at a heating rate of 10 K/min. The total organic content was determined from the mass loss occurring between 110 to 600 °C. The total organic content was then used to calculate the grafting density based on the core diameter established by TEM and the known molecular weights of nitrodopamine

and PEG. The grafting density (σ) was calculated using Equation 1, where the moles of ligand (n_{ligand}) were determined from the mass loss detected by TGA and the ligand molecular weight, N_A is the Avogadro number, the total number of NPs (N_{NPs}) was calculated from the TGA inorganic residue and the mass of a single nanoparticle (ρ = 5.24 g/cm^3) and the surface area of a single nanoparticle (A_{NP}) was obtained from TEM data. Mass loss of samples (organic content) against temperature were measured and plotted according to TGA data.

$$\sigma = \frac{Ligand\ moles\ grafted\ onto\ NPs}{Total\ surface\ area\ of\ NPs} = \frac{nligand\ .\ NA}{NNPs\ .ANP}$$

Equation.1) Ligand grafting density on nanoparticles surface calculation equation

3.10 Dynamic light scattering (DLS)

3.10.1 Colloidal Stability

DLS measurements were performed with a Malvern Nano-ZS (Malvern Instrument Ltd, UK) equipped with a 633 nm laser and operating in a backscattering mode (scattering angle of 173 °) at 20 °C. Three measurement runs were performed, and the average values of intensity, number and volume were taken for graphical analysis of the data. For the colloidal stability tests at RT all the NP samples were prepared at a concentration of 0.5 mg/mL in water or in PBS solution in 10-day intervals for a total duration of 40 days.

3.10.2 Protein interaction

DLS measurements were conducted on SPION samples purified by dialysis (0.5 mg). The samples were dissolved in 1 mL PBS containing 1 mg BSA (bovine serum albumin) and incubated at 37 °C for 1 h to investigate if the NPs aggregate upon nonspecific protein adsorption.

4. Results and Discussion

4.1 Synthesis of SPIONs

Spherical, monodisperse, and single-crystalline superparamagnetic iron oxide nanoparticles were synthesized using the thermal decomposition of $Fe(CO)_5$ (heat-up) for <15 nm NP cores[53] and thermal decomposition of $Fe(OA)_3$ (hot-injection) for >15 nm core sizes.[54, 68] The NP size could be precisely tuned in the range of 3−15 nm without any further size selection process by varying reactants ratio, temperature, and time of reaction. Five batches of different sizes with narrow size distribution were selected for further experiments. TEM images and size distribution graphs of selected batches are indicated in figure 9 and table 1(also see Appendix). The obtained NPs were characterized by low- and high-resolution TEM. Figure 9 shows TEM micrographs of monodisperse iron oxide cores and size distribution graphs calculated with Pebbles by evaluation of 250-1200 NPs from HR-TEM micrographs of the respective batches.

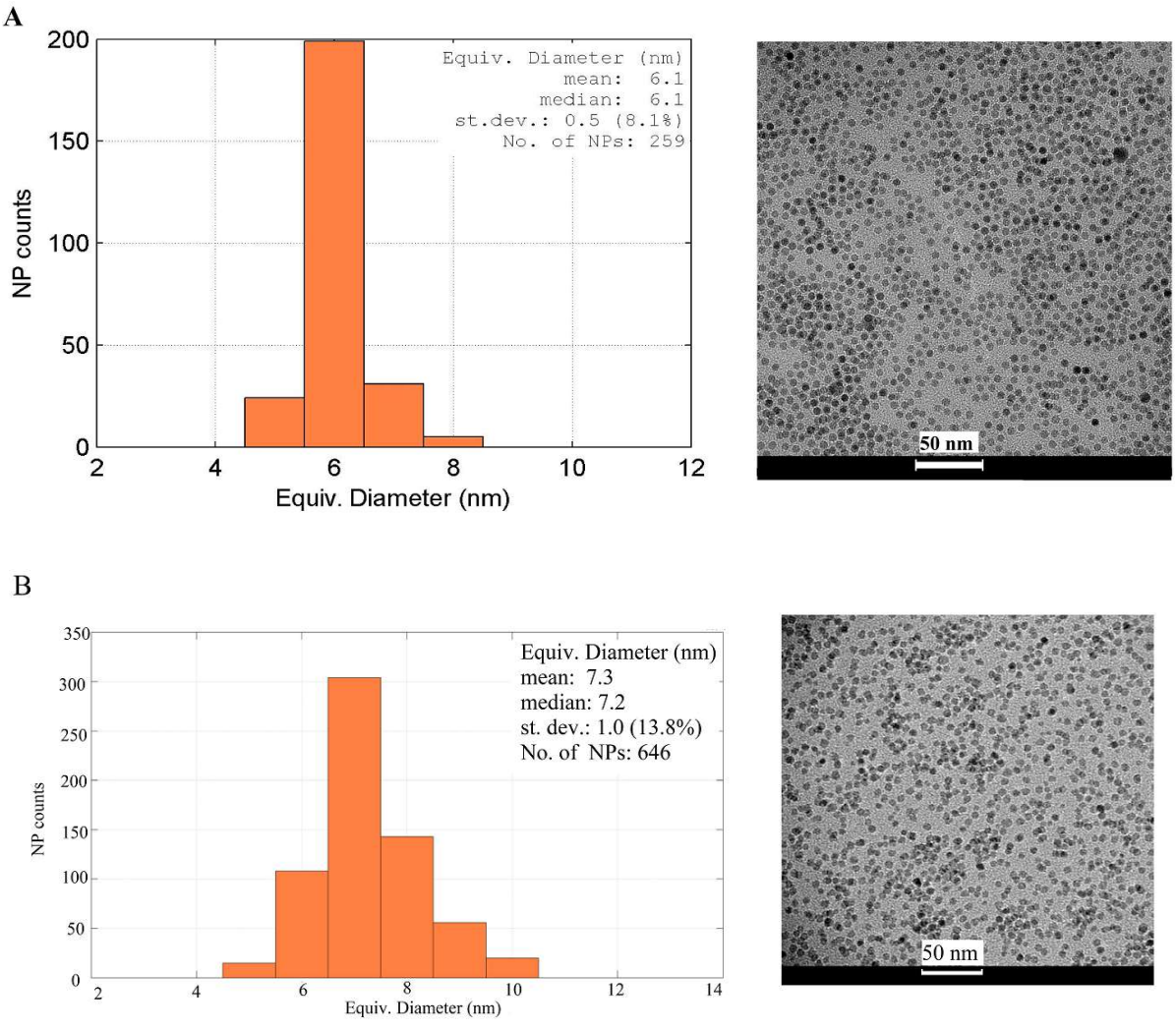

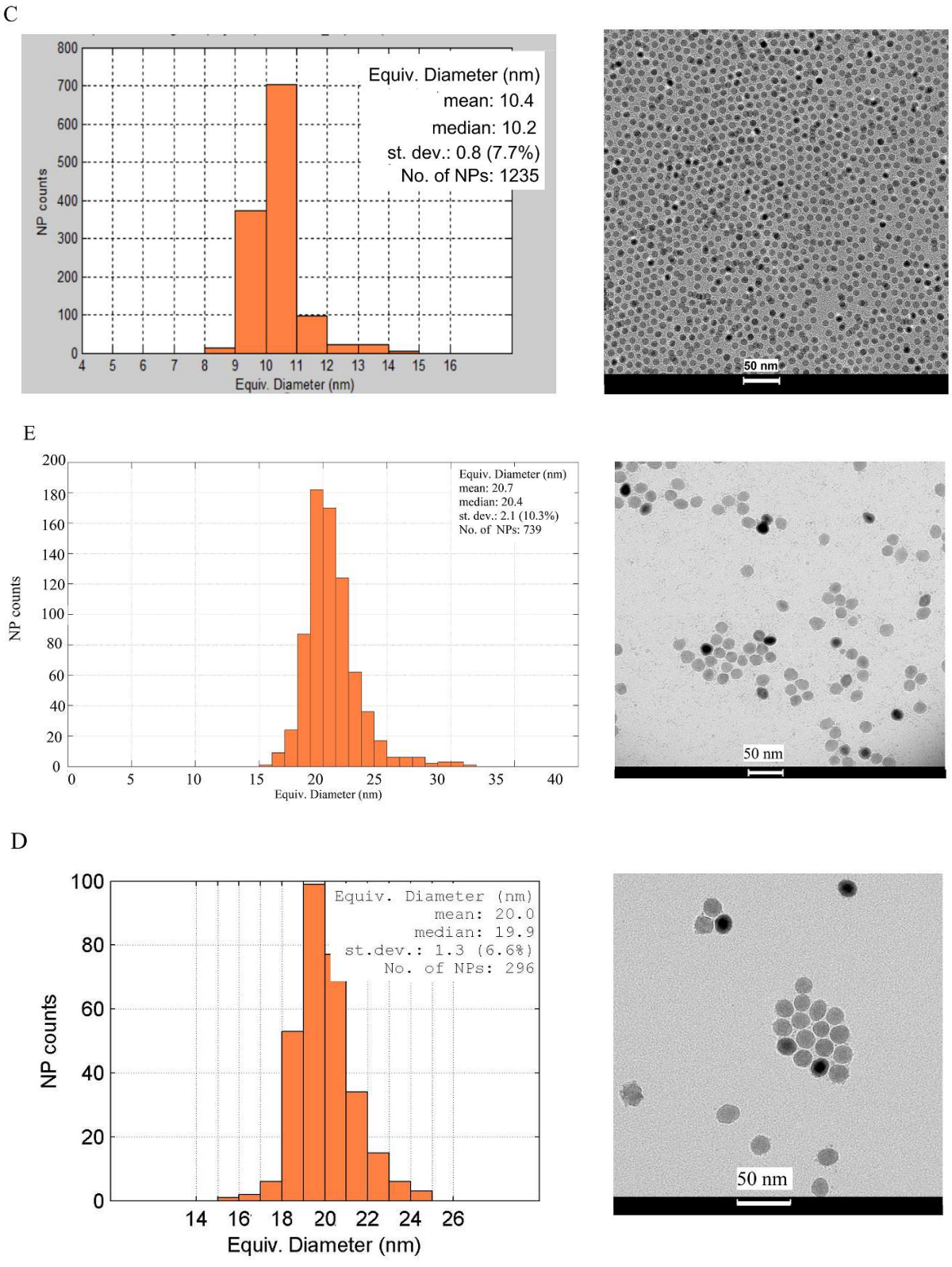

Figure 9: Transmission electron microscope images and size distribution graphs of synthesized oleic acid capped iron oxide nanoparticles that were air-dried on a carbon film supported Cu grid, A) 6.1 nm, B) 7.3 nm, C) 10.4 nm, D) 20 nm, E) 20.7 nm. Micrographs indicate that NPs are uniform and monodisperse in particle size distribution.

Table 1) Synthesised nanoparticles mean size and standard deviation of SPION core size distributions.

Synthesis method	Mean size (nm)	Standard deviation (%)
heat-up	6.1	8.1
heat-up	7.3	13.8
heat-up	10.4	7.7
hot-injection	20	6.6
hot-injection	20.7	10.3

4.2 SPIONs Functionalization and purification

Surface modification of samples was done by adapting previously developed stripping-regrafting with adding a step of solvent-free melt grafting[72] (Figure 10) and melt direct ligand exchange[74] methods.

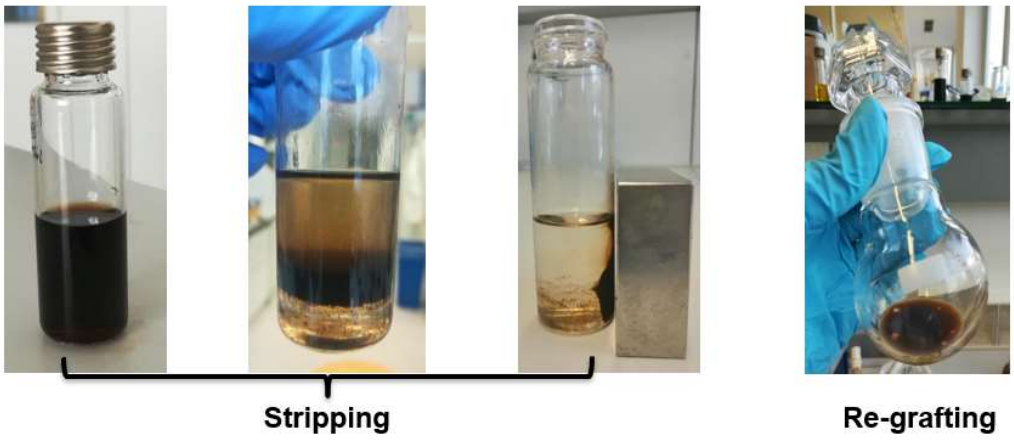

Figure 10: Stripping and regrafting of nanoparticles. Stripping the SPIONs from the initial oleic acid capping agent was performed by using KF-18-crown-6 complex. In regrafting stage, the ligand of choice which herein was PEG-NDA, placed on SPIONs surface in DMF as solvent.

Replacement of oleic acid with PEG-NDA on the nanoparticle core surface was performed in the presence of a large excess of PEG in order to ensure fast and full ligand replacement

and to provide a baseline of free PEG to allow for the evaluation of different techniques to remove free, unreacted dispersant. The separation of all excess free, unattached polymer ligand after grafting is challenging. To compare different purification methods that have been applied for core–shell nanoparticle preparation, we performed dialysis (Figure 11A), membrane centrifugation (Figure 12), precipitation with magnetic decantation (Figure 11B) and quantitatively evaluated their efficiency. The different methods were compared on their ability to remove excess PEG to a stable value determined by TGA and their effect on nanoparticle stability.

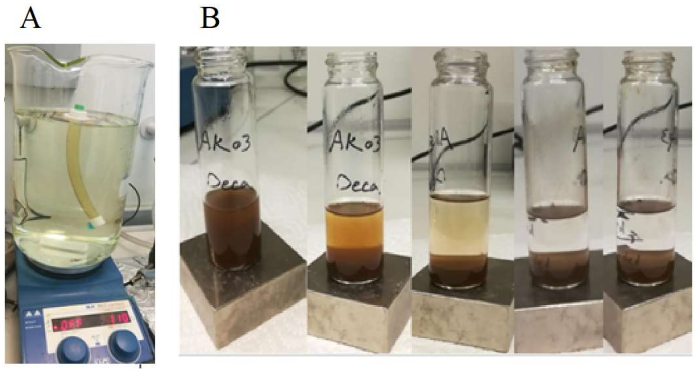

Figure 11: A) SPION purification from excess of unbound ligand via dialysis against water for 72 hours, B) magnetic decantation purification method using petroleum benzene and ethanol.

Figure 12: A) Amicon filter centrifugation steps, with proceeding the experiment effluents indicate decrease in darkness which means lower concentration of free ligand passed through the membrane, B) at the end of 12 centrifugation steps the sample remained stable and without any visible aggregation C) Amicon membrane centrifugation method: Effluents of different centrifugation steps indicating a descending trend in PEG-NDA concentrations through reaction between free PEG-NDA and sodium hydroxide which leads to a visible pink colour with darker colours indicating higher amounts of PEG-NDA.

4.3 TGA results and grafting density

The grafting density of ligands on the nanoparticle surface was evaluated by thermogravimetry analysis. For grafting density calculations, the total organic content (TOC) of the nanoparticle samples was determined as the mass loss fraction from 100 to 650 °C above which iron oxide oxidizes, and converted to the dispersant grafting density by using the known molecular weight of PEG-NDA, the average iron oxide core area determined by TEM, and a core density of 5.17 g/cm^3 according to Equation 1.

Table 2) TGA results for dialyzed particles with MWCO 1000 kDa membrane after 72 h. Grafting density of PEG-NDA after stripping was estimated according to the surface area of the SPIONs estimated by TEM and the total organic content measured by TGA (mass loss in 100 °C – 650 °C), and iron oxide core density.

SPION (nm)	**Mass loss %**	**Grafting Density (chain/nm^2)**
6.1	67.3	1.26
7.3	61	1.15
10.4	52.9	1.1
20	28.5	0.8
20.7	50.4	2.1
20.7(direct ligand exchange)	59.2	3.01

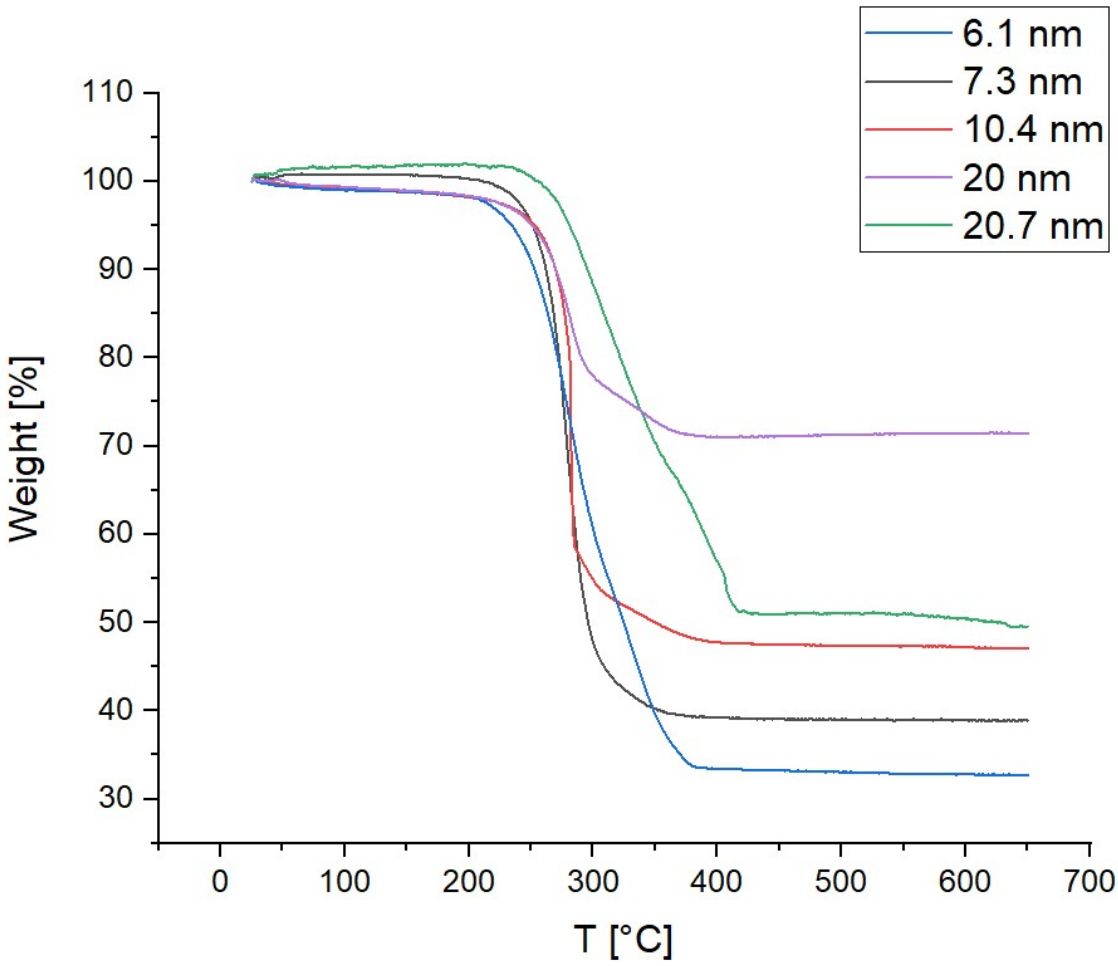

Figure 13: TGA curves, showing nanoparticle samples mass loss vs. temperature for the samples functionalised by stripping-regrafting and purified through dialysis for 72 hours.

The TGA results with corresponding PEG-NDA grafting density for dialysis are summarized in table 2 and Figure 13, indicating reasonable grafting densities of ~1 PEG-NDA polymer per square nm of NP surface after dialysis against distilled water in a 1000 kDa membrane for 72 hours. Dialysis must be performed with membranes having a pore size sufficiently large to allow diffusion of the dispersant through the pores. By using cellulose-based membranes with a MWCO of 1000 kDa, NPs will be retained in the dialysis tube while free PEG-NDA with a hydrodynamic size of ~4 nm [92] presumably is removed from the dispersion. No visible aggregation was observed after 72 hours of dialysis, which is an indication of nanoparticle stability in water. The visually observed stability is better than in previous studies, in which nanoparticles aggregated and precipitated out of solution through when subjected to similar purification protocols.[74]

For PEGylated NPs, a grafting density of 1 chain/nm^2 is considered a promising result, leading to the formation of stable colloids in biological media, which means less interaction between the nanoparticle surface and the surrounding media and less detection by the immune system.[69]

Grafting densities around 1 chain/nm^2 is in good agreement with a packing density of PEG-NDA polymer ligand.[70] Grafting density of 1-1.5 PEG chain/nm^2 on superparamagnetic spherical iron oxide nanoparticles with 25 nm diameter has been reported and tested positively for colloidal stability and cytotoxicity.[93]

Table 2 includes the total organic content and calculated grafting densities of samples prepared through modified stripping-regrafting and purified by 72 hours dialysis in MWCO 1000 kDa membrane against ultra-pure water. Direct ligand exchange led to a measured grafting density of 3.01 chains/nm^2 and visible aggregation inside the dialysis tube after 72 hours. These results are inconsistent with reports in the literature, which show much lower grafting densities with this method, but also report dialysis of similarly PEG-grafted nanoparticles to lead to a loss of colloidal stability and sample by dialysis. We, therefore, considered this combination of methods ineffective for the complete removal of free dispersant.[74]

Interestingly, the modified stripping and regrafting approach resulted in grafting densities of ~1 chain/nm^2. The threshold for hydrated PEG grafting density on iron oxide nanoparticles is affected by PEG volume (coil size) and seemed to be 0.5-1 PEG/nm^2[50, 70], meaning that for higher grafting densities removal of solvent that swells the ligands in the shell is required.

Different grafting densities of PEG on the SPION surface were previously compared and grafting densities of ~1 chain/nm^2 showed efficient blood circulation time and hence the retention of the stealth property of PEGylated nanoparticles with PEG(5 kDa).[94] Moreover, grafting of ~1 chain/nm^2 of polyoxazoline ligands on superparamagnetic iron oxide nanoparticles with 9 nm diameter were reported to produce stable core-shell nanoparticles.[95]

Therefore, the grafting density of ~1 chaun/nm^2 is known to correspond to excellent properties in terms of stability in biological suspensions,[70, 93, 96] and it is a promising result to reach the aim of the project. However, this method comes with the drawback that

the excess PEG ligand cannot be recovered as it gets lost during dialysis. 10 mL of sample is dialysed against 4 L of water, which is replaced two times per day over 72 hours. Therefore, it is not feasible to recycle PEG ligands passing through the membrane into the dialysis water.

Table 3) Mass losses and calculated grafting densities for samples of 10.4 nm size under different rounds of Amicon filter centrifugation

Centrifugation step	**Mass loss %**	**Grafting Density (chain/nm^2)**
0	88.99	8.44
5	31.25	0.47
7	29.95	0.45
10	28.57	0.42
12	30.77	0.46

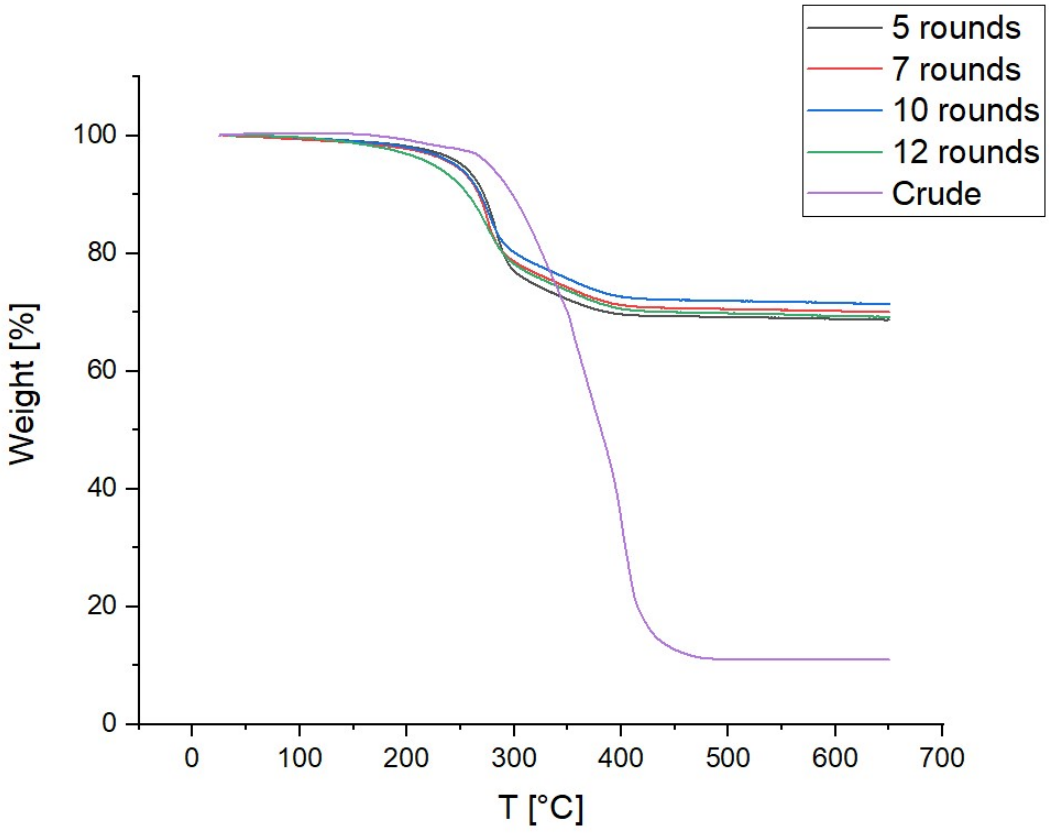

Figure 14: TGA graphs showing mass loss trends of different steps of membrane centrifugation purification method performed on 10.4 nm size nanoparticles by using a 100 kDa Amicon-Ultra15 membrane centrifugation filter unit.

Amicon membrane centrifugation is a promising alternative method regarding the possibility of recycling excess ligands because the excess ligand is collected in a small volume at high ligand concentration, which makes it easier to recycle the unattached free PEG ligands. Membrane centrifugation with Amicon 100 kDa centrifugation unit at 4500 g for 12 rounds resulted in grafting densities as low as 0.5 chain/nm^2 (Table 3 and Figure 14) of NPs surface. Low grafting densities (around 0.5) were related to over-purification. Due to a low grafting density of the ligand (around 0.5), the particles were poorly dispersible in water or PBS for any other measurement such as DLS. Additionally, another study showed that this method failed to purify the PEGylated SPIONs by direct ligand exchange, probably for similar reasons.[74] In the previous research, 15 rounds of Amicon filter centrifugation of melt grafted SPIONs showed a constant decrease in grafting density and colloidal instability of SPIONs. In this work, SPIONs showed neither significant a reduction of the grafting density with the number of repetitions nor visible aggregation during 12 steps of filtration. This shows that this method cannot be considered as a promising purification approach.

Consequently, the most promising grafting densities were reached through a modified stripping-regrafting method, which resulted in higher grafting densities. In this approach, stripping of oleate-coated NPs was performed as described before, but in order to decrease ligand coil size and achieve higher grafting of ligand on the nanoparticle surface, the regrafting step was modified. The modified regrafting process consisted of two steps, 3 hours of sonication of the NPs and PEG-NDA in the presence of DMF as solvent followed by a second step of removing the DMF through evaporation-lyophilization and melting the solvent-free sample for 90 min in 110 °C. It seems that DMF solvent shows a dual effect in the regrafting of ligand on the surface of the bare nanoparticles. On the one hand, it helps to disperse the particles and improve the mixing of particles and ligands. On the other hand, it swells the ligand and makes it bulky, which leads to steric hindrance and, therefore, lower grafting density on the nanoparticle surface. Due to the second reason, we attempted to remove solvent after mixing particles and ligands through evaporating DMF using a Rotavapor and 48 h lyophilization. This decreases the size of the polymer coils by removing the solvent that swells them, while the grafting of the cores with PEG during the first step ensures that they are reasonably dispersed and mixed. The more compact polymers will pack more densely on the surfaces of the NPs because of reduced steric hindrance, which should result in higher grafting densities. All nanoparticle batches were then stripped-regrafted by this method and went through further experiments to prove the efficiency of this protocol.

Table 4) TGA results for magnetic separation plus AL_2O_3 addition methods performed on NPs of 6.1 nm core size

SPION Size (nm)	**Purification Method**	**Mass loss (%)**	**Grafting Density (Chain/nm^2)**
6.1	Magnetic Decantation	91.7	6.8
6.1	Magnetic Dec. plus Al_2O_3 Addition	87.3	4.2

Magnetic decantation resulted in a very high grafting density of 6.8 chain/nm^2 (Table 4). This large number of ligands cannot be adhered firmly on a square nanometre of SPIONs surface and demonstrates that all excess dispersant was not removed by this method.

Although, magnetic separation was previously reported to result in reasonable grafting densities around 1 chain/nm^2 of PEG-NDA on SPION,[74] it clearly failed to remove the excess dispersant in the present study. Additionally, it was tried to combine the method with affinity-based methods to further decrease the grafting density of produced nanoparticles. Therefore, aluminium oxide beads were added to SPION dispersions after magnetic decantation, but the resulting grafting density was still high (4.2 chain/nm^2) after 5 rounds of separation of supernatant and addition of fresh aluminium oxide beads. As this grafting density is slightly higher than the expected bonding limit set by the number of surface iron cation binding sites, it is reasonable to believe that also this purification method was unsuccessful in removing all excess dispersant. Hence, the purification method was considered inefficient or requiring further optimization.

4.4 DLS Analysis

4.4.1 Hydrodynamic Size

Dynamic light scattering (DLS) measurements of dialyzed particles were performed to analyse hydrodynamic diameter and behaviour of the particles in Milli-Q water and PBS. A concentration of 0.5 mg/mL was used for all samples. Number-weighted size distributions acquired by DLS, depicted in Figure 15 (also see Appendix), was used to show changes in hydrodynamic diameter in nm. All the graphs showed single peaks, which indicate the narrow size distribution and high colloidal stability of SPIONs in PBS and water.

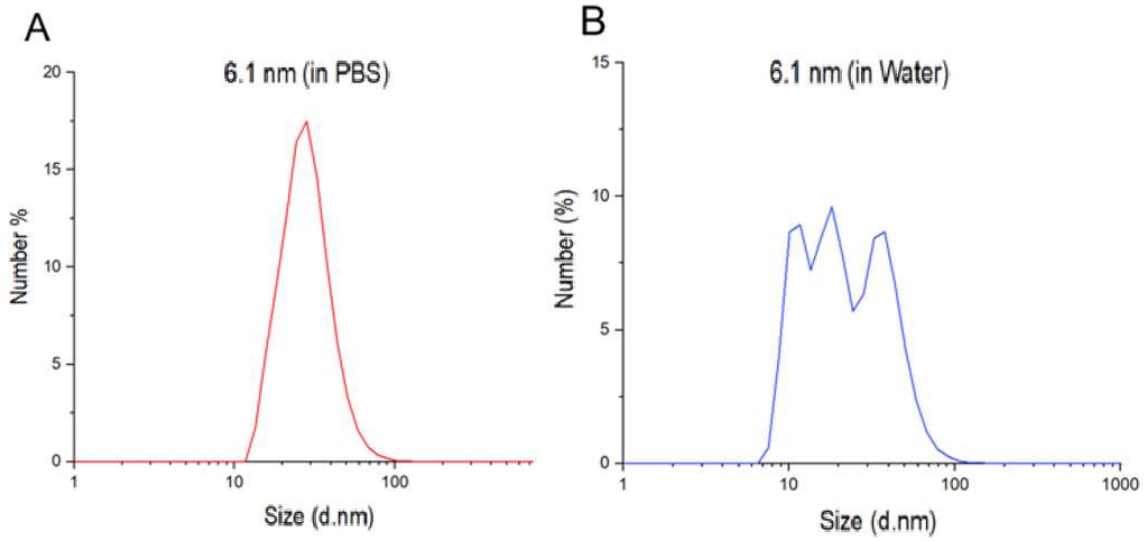

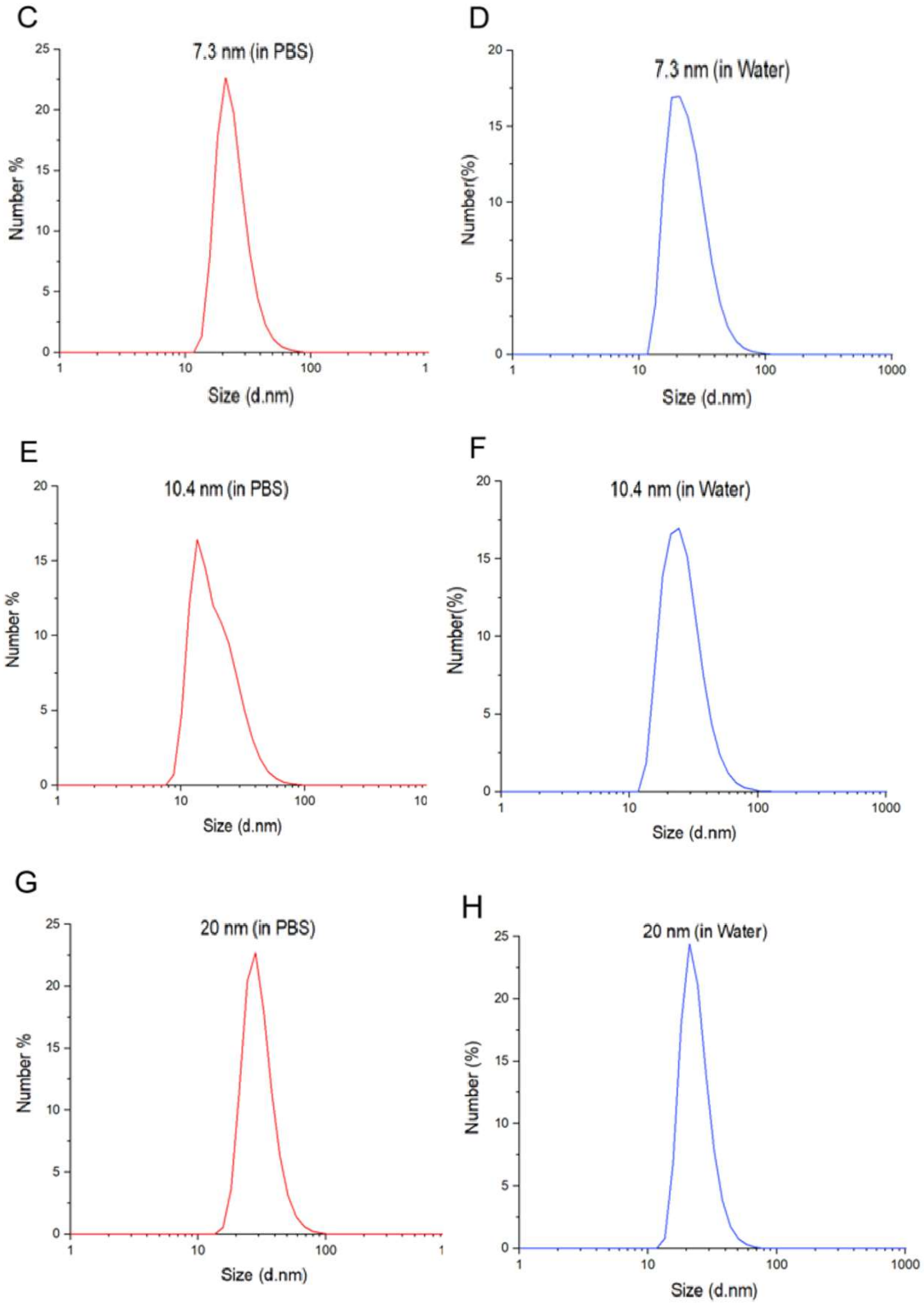
C
7.3 nm (in PBS)
Number %
Size (d.nm)
D
7.3 nm (in Water)
Number(%)
Size (d.nm)
E
10.4 nm (in PBS)
Number %
Size (d.nm)
F
10.4 nm (in Water)
Number(%)
Size (d.nm)
G
20 nm (in PBS)
Number %
Size (d.nm)
H
20 nm (in Water)
Number (%)
Size (d.nm)

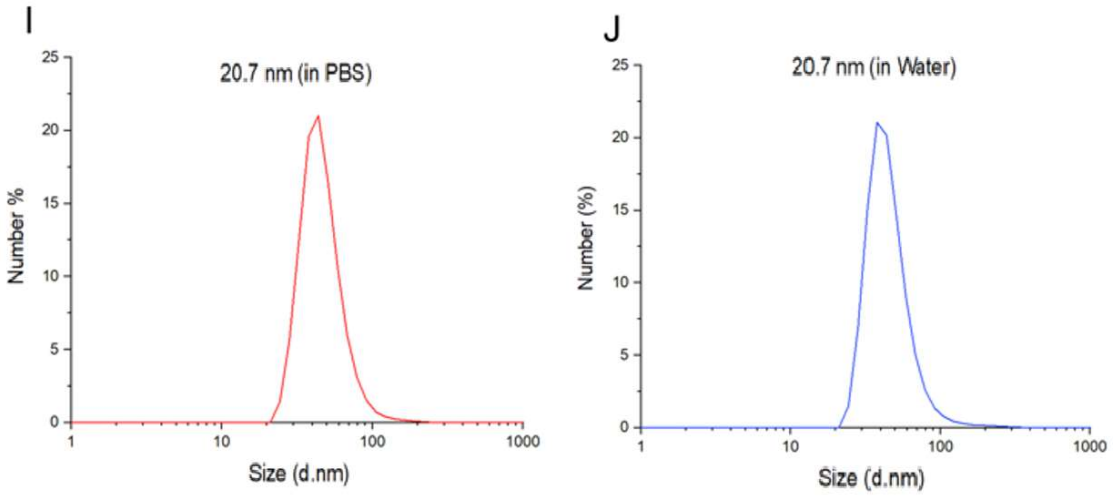

Figure 14: Hydrodynamic size measurements using DLS of dialyzed iron oxide nanoparticles. The samples were *dissolved in MilliQ water and PBS with* a *particle concentration of 0.5 mg/mL. Number*-weighted size distributions *of DLS* measurements are *used to show changes in hydrodynamic diameter (DH) in nm. The number-weighted size distributions* are depicted for different SPION sizes: *A) 6.1 nm* core size *SPIONs* dispersed in *PBS, B) 6.1nm SPIONs in water, C) 7.3nm SPIONs in PBS, D) 7.3nm SPIONs in water, E) 10.4 nm in PBS, F) 10.4nm in water, G) 20 nm in PBS, H) 20nm in water, I) 20.7nm in PBS, J) 20.7 nm in water.*

4.4.2 Long Term Colloidal Stability

The long-term stability of polymer ligand grafted SPIONs prevents NPs from being aggregated in proper solvent and makes them ideal for long term storages. Long-term colloidal stability of dialyzed SPIONs was investigated with DLS in Milli-Q water and PBS (Figure 16). All nanoparticle dispersions in PBS were stable except for the 20.7 nm particles, which started to form large aggregates after 20 days. This is a surprising result given the high apparent grafting density of 2.1 chain/nm^2 measured for this sample. Large cores should require a thicker but less densely grafted shell for colloidal stability than smaller particles. Thus, it is either possible that a higher molecular weight dispersant should have been chosen to fully counter the van der Waals attraction of the cores or that the purification of this sample was incomplete and the grafting density overestimated. All other samples with a grafting density of ~1 chain/nm^2 showed promising colloidal stability when suspended in PBS, and almost no aggregation was observed within 40 days.

20.7 nm particles showed a higher hydrodynamic diameter and higher colloidal stability in water than in PBS, compared to other SPIONs. As experiments continued, the particles started to show a lower hydrodynamic diameter and become stable in the long term. One possible reason could be the precipitation of aggregates of particles with too low grafting density over time. This would be consistent with the hypothesis above that the average

grafting density was overestimated for this sample. All other samples with a grafting density of ~1 ligand/nm^2 showed promising colloidal stability when suspended in water, and almost no aggregation was observed within 40 days.

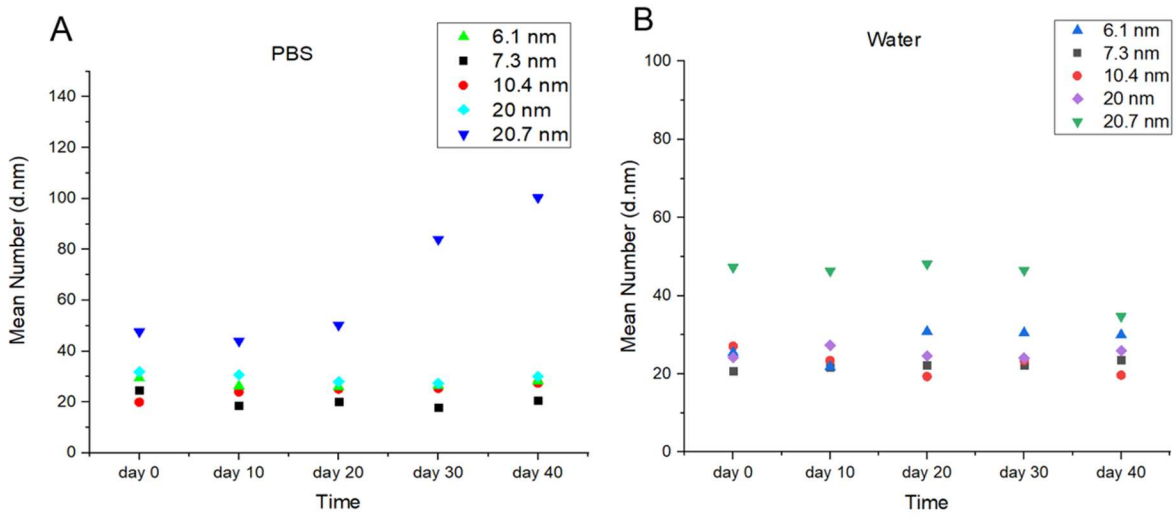

Figure 15: Long-term colloidal stability of dialyzed SPIONs experiment performed in water and PBS. Samples were dissolved in MilliQ water and PBS with particle concentration of 1 mg/mL. Mean number data of DLS is used to show changes in hydrodynamic diameter in nm hydrodynamic size details of nanoparticles during a period of 40 days, being measured in 10 days intervals in A) PBS and B) water.

4.4.3 Protein Interaction

Excellent biocompatibility is one of the fundamental requirements for an efficient contrast agent. Hence, their interaction with serum proteins is crucial. Since iron oxide nanoparticles are to be injected to biological systems and remain suspended and stable, the colloidal stability of all dialyzed samples were evaluated after being incubated in PBS containing 1 mg/mL bovine serum albumin (BSA). Albumin is the most abundant protein in blood. The SPIONs were incubated in the BSA solution for 1 h at 37°C. After 1h of incubation, the interaction between SPIONs and BSA was investigated by DLS (Figure 17, also see Appendix).

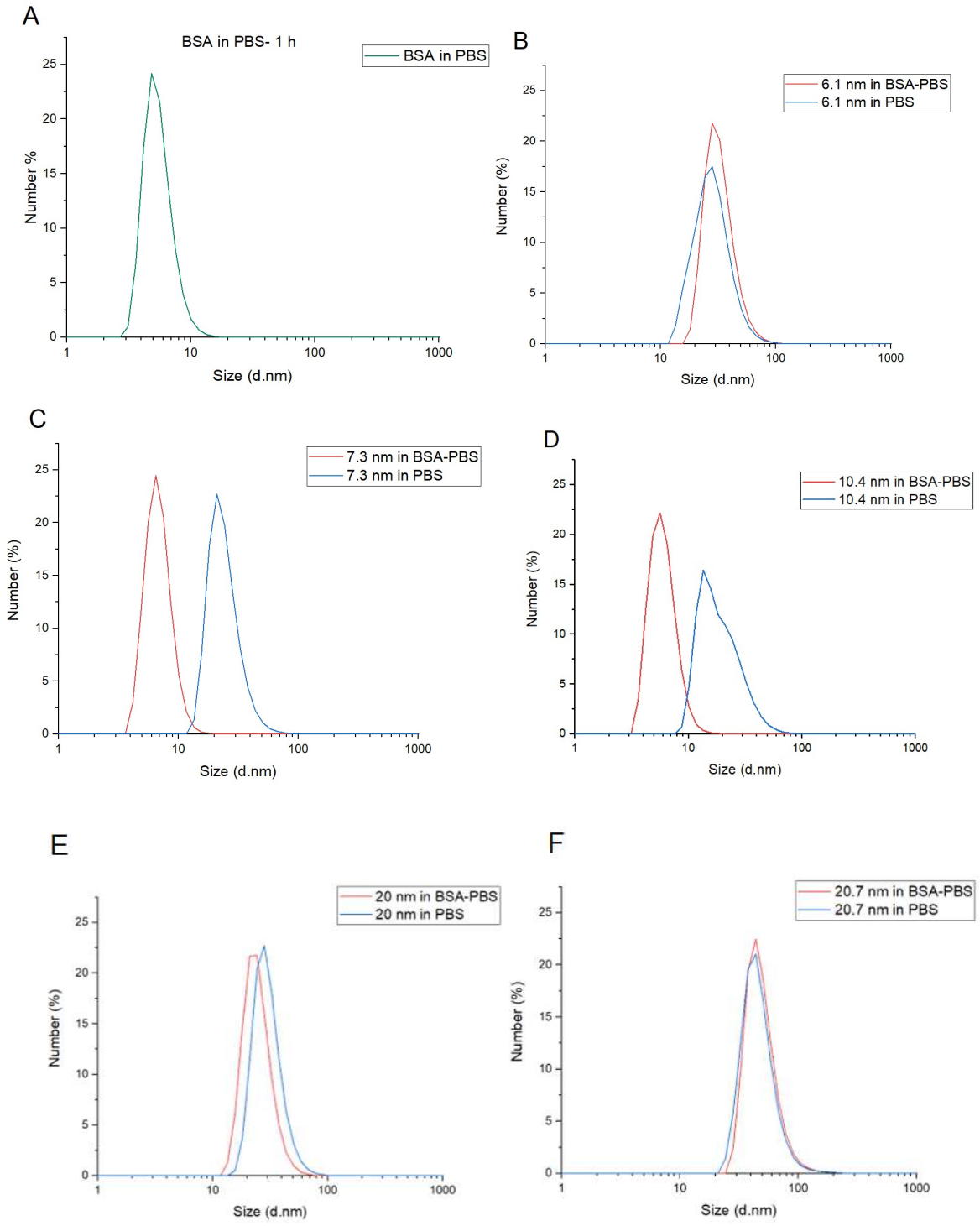

Figure 16: Protein interaction curves for different SPIONs (0.5mg/ml) size, A) pure bovine serum albumin in phosphate buffered saline, B) 6.1 nm, C) 7.3nm, D) 10.4 nm, E) 20 nm, and F) 20.7 nm SPIONs in PBS with 1mg/mL BSA, indicating no visible aggregation in bovine serum albumin.

Most samples showed a significant change in hydrodynamic size and size distribution in comparison to those in pure PBS. The signal related to BSA centered around 5 nm is not observable for all nanoparticle samples. While the abundance of the BSA compared to the

nanoparticle, makes the peak visible or shifts the convoluted peak of BSA and nanoparticles to lower hydrodynamic diameter for small nanoparticles, it is masked by the much stronger scattering signal of large nanoparticles. Importantly, there is no shift to larger hydrodynamic size for any sample after mixing with BSA. The results show that the interaction with highly concentrated protein solutions does not lead to aggregation of the PEGylated particles; all SPION samples possessed high grafting densities (>0.8 chains per nm^2 of PEG-NDA) and remained stable in bovine serum without aggregation. It was shown in previous research [68] that serum proteins are able to interact with and bind to the core of iron oxide NPs that are not densely grafted (<0.5 of PEG-5 kDa per nm^2) and lead the particles to precipitate, while densely grafted NPs are efficiently shielded and hence remained suspended. Covering of nanoparticles with a shell of organic ligands prevent them from specific binding and interacting with proteins in biological media and keep them colloidally stable.[97] Generally, upon entering of nanoparticles into the biological media, they start to interact with biomolecules, including proteins, which leads to the formation and development of a "protein corona" around nanoparticles.[98, 99] Thus, these could be ascribed to nonspecific binding or adsorption and protein corona formation around SPIONs, which did not lead to their aggregation.

4.5 ^{1}H-NMR

To make sure that regrafted SPIONs are oleic acid free, nuclear magnetic resonance (NMR) was used to quantify the composition of the surface coating of the SPIONs after purification. Given that iron oxide nanoparticles change the relaxation time and expand NMR spectrum, the particle cores were removed by dissolving in concentrated HCl, and the covering ligand was extracted with chloroform. ^{1}H NMR spectra of the extracted ligand (Figure 18) showed no characteristic signal from allylic protons of oleic acid in the range of 5-6 ppm chemical shifts, which confirms the absence of the oleic acid polymer ligand on the surface of SPIONs. The absence of hydrophobic hydrocarbon around the core will guarantee the presence of a higher number of the water molecules close to the SPION cores, which is required for a high MRI signal, as well as likely contribute to the high colloidal stability that was observed of the regrafted nanoparticles.

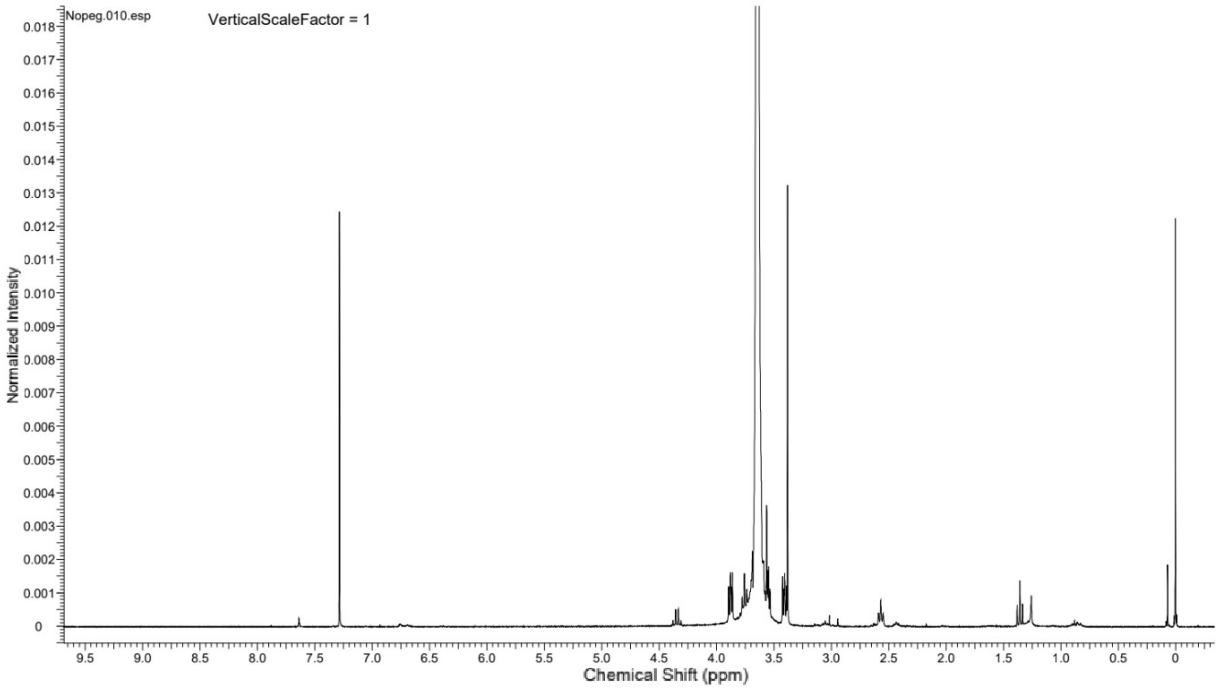

Figure 17: NMR profile of isolated shell from PEGylated SPIONs, signals associated with allylic protons of oleic acid between 5-6 ppm were not observed therefore, stripping of NPs was successfully performed.

5. Conclusion

Synthesis of nanoparticles with very narrow size distribution has been intensively pursued because of their technological and scientific importance. In this study, it was shown that replacing of oleic acid with a PEG(5 kDa) polymer ligand anchored with nitrodopamine on the surface of the SPIONs leads to the successful transformation of hydrophobic to hydrophilic nanoparticles. The PEGylated SPIONs demonstrated excellent stability in water and PBS monitored over a 40-day period. Uniquely, it could be demonstrated that the stripping and regrafting method led to no traces of oleic acid in the shell of the nanoparticles. The PEG-grafted SPIONs were stable in the presence of the most abundant protein in blood serum, BSA. Purification is a critical step in obtaining desirable NP despersions. Based on the results of this study, membrane dialysis is a promising method for purification of SPIONs coated with PEG, resulting to grafting densities ~1 chain/nm^2, which is considered a favourable grafting density for application as contrast agent. The achieved grafting density is sufficient to keep the resulting hydrophilic NPs colloidally stable. However, this method is not very attractive to recover the separated free ligands and is unsuitable for large scale-up. Membrane centrifugation resulted in grafting densities ~0.5 chain/nm^2 and could be an efficient method for recycling excess ligand because of small quantities of collected eluates. However, this grafting density is lower than desired for full colloidal stability. The other tested purification methods (magnetic decantation and affinity column purification) failed to efficiently remove the excess dispersant. The purified SPIONs are promising candidates for MRI studies to practically investigate their capability of being applied as contrast agents in medicine. For that, other characterization methods such as relaxivity measurements should be performed.

6. References

1. 18401, I.T., *Nanotechnologies — Plain language explanation of selected terms from the ISO/IEC 80004 series*. 2017.
2. Kuhlbusch, T.A., et al., *Nanoparticle exposure at nanotechnology workplaces: a review*. Particle and fibre toxicology, 2011. **8**(1): p. 22.
3. Lead, J.R. and E. Smith, *Environmental and human health impacts of nanotechnology*. 2009: John Wiley & Sons.
4. Filella, M., *Colloidal properties of submicron particles in natural waters.* IUPAC series on analytical and physical chemistry of environmental systems, 2007. **10**: p. 17.
5. Fageria, P., S. Gangopadhyay, and S. Pande, *Synthesis of ZnO/Au and ZnO/Ag nanoparticles and their photocatalytic application using UV and visible light.* Rsc Advances, 2014. **4**(48): p. 24962-24972.
6. Zhang, Y., et al., *Preparation of thiol-modified Fe3O4@ SiO2 nanoparticles and their application for gold recovery from dilute solution.* Separation and Purification Technology, 2013. **116**: p. 391-397.
7. Colvin, V.L., *The potential environmental impact of engineered nanomaterials.* Nature biotechnology, 2003. **21**(10): p. 1166-1170.
8. Khan, S.B., et al., *Exploration of CeO2 nanoparticles as a chemi-sensor and photo-catalyst for environmental applications.* Science of the total Environment, 2011. **409**(15): p. 2987-2992.
9. Westerhoff, P., et al., *Low risk posed by engineered and incidental nanoparticles in drinking water.* Nature nanotechnology, 2018. **13**(8): p. 661-669.
10. Guo, H. and A.S. Barnard, *Naturally occurring iron oxide nanoparticles: morphology, surface chemistry and environmental stability.* Journal of Materials Chemistry A, 2013. **1**(1): p. 27-42.
11. Barnard, A.S. and H. Guo, *Nature's Nanostructures*. 2012: CRC Press.
12. Zhang, H., J.R. Rustad, and J.F. Banfield, *Interaction between water molecules and zinc sulfide nanoparticles studied by temperature-programmed desorption and molecular dynamics simulations.* The Journal of Physical Chemistry A, 2007. **111**(23): p. 5008-5014.
13. Wagner, S., et al., *Spot the difference: engineered and natural nanoparticles in the environment—release, behavior, and fate.* Angewandte Chemie International Edition, 2014. **53**(46): p. 12398-12419.
14. Rebodos, R.L. and P.J. Vikesland, *Effects of oxidation on the magnetization of nanoparticulate magnetite.* Langmuir, 2010. **26**(22): p. 16745-16753.
15. Vaseem, M., et al., *Iron Oxide Nanoparticle-Based Magnetic Ink Development for Fully Printed Tunable Radio-Frequency Devices.* Advanced Materials Technologies, 2018. **3**(4): p. 1700242.
16. Parker, F., et al., *Spin-glass behavior of spinel iron oxide particles on iron metal particle recording media.* Journal of applied physics, 1995. **77**(11): p. 5853-5864.
17. Liang, Y.-Y., et al., *Polysaccharide-modified iron oxide nanoparticles as an effective magnetic affinity adsorbent for bovine serum albumin.* Colloid and Polymer Science, 2007. **285**(11): p. 1193-1199.
18. Gong, J.-L., et al., *Copper (II) removal by pectin–iron oxide magnetic nanocomposite adsorbent.* Chemical Engineering Journal, 2012. **185**: p. 100-107.
19. Kim, T., et al., *Size-controlled Pd nanoparticle catalysts prepared by galvanic displacement into a porous Si-Iron oxide nanoparticle host.* ACS nano, 2017. **11**(3): p. 2773-2784.
20. Brullot, W., et al., *Versatile ferrofluids based on polyethylene glycol coated iron oxide nanoparticles.* Journal of Magnetism and Magnetic Materials, 2012. **324**(11): p. 1919-1925.

21. Berry, C.C. and A.S. Curtis, *Functionalisation of magnetic nanoparticles for applications in biomedicine.* Journal of physics D: Applied physics, 2003. **36**(13): p. R198.
22. Babes, L., et al., *Synthesis of iron oxide nanoparticles used as MRI contrast agents: a parametric study.* Journal of colloid and interface science, 1999. **212**(2): p. 474-482.
23. Arias, L., et al., *Iron oxide nanoparticles for biomedical applications: A perspective on synthesis, drugs, antimicrobial activity, and toxicity.* Antibiotics, 2018. **7**(2): p. 46.
24. Alwi, R., et al., *Silica-coated super paramagnetic iron oxide nanoparticles (SPION) as biocompatible contrast agent in biomedical photoacoustics.* Biomedical optics express, 2012. **3**(10): p. 2500-2509.
25. Wu, W., et al., *Recent progress on magnetic iron oxide nanoparticles: synthesis, surface functional strategies and biomedical applications.* Science and technology of advanced materials, 2015. **16**(2): p. 023501.
26. Maeng, J.H., et al., *Multifunctional doxorubicin loaded superparamagnetic iron oxide nanoparticles for chemotherapy and magnetic resonance imaging in liver cancer.* Biomaterials, 2010. **31**(18): p. 4995-5006.
27. Dadfar, S.M., et al., *Iron oxide nanoparticles: Diagnostic, therapeutic and theranostic applications.* Advanced drug delivery reviews, 2019. **138**: p. 302-325.
28. Wáng, Y.X.J. and J.-M. Idée, *A comprehensive literatures update of clinical researches of superparamagnetic resonance iron oxide nanoparticles for magnetic resonance imaging.* Quantitative imaging in medicine and surgery, 2017. **7**(1): p. 88.
29. Mahmoudi, M., et al., *Superparamagnetic iron oxide nanoparticles (SPIONs): development, surface modification and applications in chemotherapy.* Advanced drug delivery reviews, 2011. **63**(1-2): p. 24-46.
30. Wahajuddin, S.A., *Superparamagnetic iron oxide nanoparticles: magnetic nanoplatforms as drug carriers.* International journal of nanomedicine, 2012. **7**: p. 3445.
31. Chertok, B., et al., *Iron oxide nanoparticles as a drug delivery vehicle for MRI monitored magnetic targeting of brain tumors.* Biomaterials, 2008. **29**(4): p. 487-496.
32. Varanasi, P., A. Fullana, and S. Sidhu, *Remediation of PCB contaminated soils using iron nano-particles.* Chemosphere, 2007. **66**(6): p. 1031-1038.
33. Shipley, H.J., K.E. Engates, and A.M. Guettner, *Study of iron oxide nanoparticles in soil for remediation of arsenic.* Journal of Nanoparticle Research, 2011. **13**(6): p. 2387-2397.
34. Elias, A. and A. Tsourkas, *Imaging circulating cells and lymphoid tissues with iron oxide nanoparticles.* ASH Education Program Book, 2009. **2009**(1): p. 720-726.
35. Kodama, R., *Magnetic nanoparticles.* Journal of magnetism and magnetic materials, 1999. **200**(1-3): p. 359-372.
36. Riaz, S., S.S. Hussain, and S. Naseem, *Structural and Magnetic Properties of Monodispersed Iron Oxide Nanoparticles for use in Magnetic Resonance Imaging.*
37. Hassellöv, M. and R. Kaegi, *Analysis and characterization of manufactured nanoparticles in aquatic environments*. 2009: John Wiley & Sons, Inc.: United Kingdom.
38. Guardia, P., A. Labarta, and X. Batlle, *Tuning the size, the shape, and the magnetic properties of iron oxide nanoparticles.* The Journal of Physical Chemistry C, 2011. **115**(2): p. 390-396.
39. Singh, N., et al., *Potential toxicity of superparamagnetic iron oxide nanoparticles (SPION).* Nano reviews, 2010. **1**(1): p. 5358.
40. Natarajan, S., et al., *Multifunctional magnetic iron oxide nanoparticles: diverse synthetic approaches, surface modifications, cytotoxicity towards biomedical and industrial applications.* BMC Materials, 2019. **1**(1): p. 2.
41. Laurent, S., et al., *Magnetic iron oxide nanoparticles: synthesis, stabilization, vectorization, physicochemical characterizations, and biological applications.* Chemical reviews, 2008. **108**(6): p. 2064-2110.
42. Gupta, A.K. and M. Gupta, *Synthesis and surface engineering of iron oxide nanoparticles for biomedical applications.* biomaterials, 2005. **26**(18): p. 3995-4021.

43. Thanikaivelan, P., et al., *Collagen based magnetic nanocomposites for oil removal applications.* Scientific reports, 2012. **2**: p. 230.
44. Kumar, A., et al., *SPION/β-cyclodextrin core–shell nanostructures for oil spill remediation and organic pollutant removal from waste water.* Chemical Engineering Journal, 2015. **280**: p. 175-187.
45. Merbach, *The Chemistry of Contrast Agents in Medical Magnetic Resonance Imaging.pdf*. 2013.
46. Kehrer, J.P., *The Haber–Weiss reaction and mechanisms of toxicity.* Toxicology, 2000. **149**(1): p. 43-50.
47. Shirmardi Shaghasemi, B., *Supermagnetic Iron Oxide Nanoparticles; Surface Modification and Application* 2017, BOKU.
48. Moore, T.L., et al., *Nanoparticle colloidal stability in cell culture media and impact on cellular interactions.* Chemical Society Reviews, 2015. **44**(17): p. 6287-6305.
49. Israelachvili, J.N., *Intermolecular and surface forces*. 2015: Academic press.
50. Lassenberger, *thesis Andrea Lassenberger_PhD Thesis.pdf*. 2017.
51. Marinin, A., *Synthesis and characterization of superparamagnetic iron oxide nanoparticles coated with silica*. 2012.
52. Hufschmid, R., et al., *Synthesis of phase-pure and monodisperse iron oxide nanoparticles by thermal decomposition.* Nanoscale, 2015. **7**(25): p. 11142-11154.
53. Hyeon, T., et al., *Synthesis of highly crystalline and monodisperse maghemite nanocrystallites without a size-selection process.* Journal of the American Chemical Society, 2001. **123**(51): p. 12798-12801.
54. Park, J., et al., *Ultra-large-scale syntheses of monodisperse nanocrystals.* Nature materials, 2004. **3**(12): p. 891-895.
55. de Mello Donegá, C., P. Liljeroth, and D. Vanmaekelbergh, *Physicochemical evaluation of the hot-injection method, a synthesis route for monodisperse nanocrystals.* Small, 2005. **1**(12): p. 1152-1162.
56. Ghosh Chaudhuri, R. and S. Paria, *Core/shell nanoparticles: classes, properties, synthesis mechanisms, characterization, and applications.* Chemical reviews, 2012. **112**(4): p. 2373-2433.
57. Tassa, C., S.Y. Shaw, and R. Weissleder, *Dextran-coated iron oxide nanoparticles: a versatile platform for targeted molecular imaging, molecular diagnostics, and therapy.* Accounts of chemical research, 2011. **44**(10): p. 842-852.
58. Cole, A.J., et al., *Polyethylene glycol modified, cross-linked starch-coated iron oxide nanoparticles for enhanced magnetic tumor targeting.* Biomaterials, 2011. **32**(8): p. 2183-2193.
59. Yue-Jian, C., et al., *Synthesis, self-assembly, and characterization of PEG-coated iron oxide nanoparticles as potential MRI contrast agent.* Drug development and industrial pharmacy, 2010. **36**(10): p. 1235-1244.
60. Larsen, E.K.U., et al., *Accumulation of magnetic iron oxide nanoparticles coated with variably sized polyethylene glycol in murine tumors.* Nanoscale, 2012. **4**(7): p. 2352-2361.
61. García-Jimeno, S. and J. Estelrich, *Ferrofluid based on polyethylene glycol-coated iron oxide nanoparticles: characterization and properties.* Colloids and Surfaces A: Physicochemical and Engineering Aspects, 2013. **420**: p. 74-81.
62. Yu, M., et al., *Dextran and polymer polyethylene glycol (PEG) coating reduce both 5 and 30 nm iron oxide nanoparticle cytotoxicity in 2D and 3D cell culture.* International journal of molecular sciences, 2012. **13**(5): p. 5554-5570.
63. Mojica Pisciotti, M.L., et al., *In vitro and in vivo experiments with iron oxide nanoparticles functionalized with DEXTRAN or polyethylene glycol for medical applications: magnetic targeting.* Journal of Biomedical Materials Research Part B: Applied Biomaterials, 2014. **102**(4): p. 860-868.

64. Wang, Y.-X.J., *Superparamagnetic iron oxide based MRI contrast agents: Current status of clinical application.* Quantitative imaging in medicine and surgery, 2011. **1**(1): p. 35.
65. Remya, N., et al., *Toxicity, toxicokinetics and biodistribution of dextran stabilized Iron oxide Nanoparticles for biomedical applications.* International journal of pharmaceutics, 2016. **511**(1): p. 586-598.
66. Amstad, E., M. Textor, and E. Reimhult, *Stabilization and functionalization of iron oxide nanoparticles for biomedical applications.* Nanoscale, 2011. **3**(7): p. 2819-2843.
67. Kumagai, M., et al., *Iron hydroxide nanoparticles coated with poly (ethylene glycol)-poly (aspartic acid) block copolymer as novel magnetic resonance contrast agents for in vivo cancer imaging.* Colloids and Surfaces B: Biointerfaces, 2007. **56**(1-2): p. 174-181.
68. Zirbs, R., et al., *Melt-grafting for the synthesis of core–shell nanoparticles with ultra-high dispersant density.* Nanoscale, 2015. **7**(25): p. 11216-11225.
69. Cruje, C. and D. Chithrani, *Polyethylene glycol density and length affects nanoparticle uptake by cancer cells.* J Nanomed Res, 2014. **1**(1): p. 00006.
70. Amstad, E., et al., *Ultrastable iron oxide nanoparticle colloidal suspensions using dispersants with catechol-derived anchor groups.* Nano letters, 2009. **9**(12): p. 4042-4048.
71. Sun, S., et al., *Monodisperse mfe2o4 (m= fe, co, mn) nanoparticles.* Journal of the American Chemical Society, 2004. **126**(1): p. 273-279.
72. Shaghasemi, B.S., et al., *Host–guest driven ligand replacement on monodisperse inorganic nanoparticles.* Nanoscale, 2017. **9**(26): p. 8925-8929.
73. Bixner, O., et al., *Complete exchange of the hydrophobic dispersant shell on monodisperse superparamagnetic iron oxide nanoparticles.* Langmuir, 2015. **31**(33): p. 9198-9204.
74. Lassenberger, A., et al., *Evaluation of high-yield purification methods on monodisperse peg-grafted iron oxide nanoparticles.* Langmuir, 2016. **32**(17): p. 4259-4269.
75. Heggie, J.C., *Magnetic resonance imaging: Principles, methods and techniques by perry sprawls.* Australasian Physical & Engineering Science in Medicine, 2001. **24**(1): p. 57-57.
76. Dale, B.M., M.A. Brown, and R.C. Semelka, *MRI: basic principles and applications*. 2015: John Wiley & Sons.
77. Muja, N. and J.W. Bulte, *Magnetic resonance imaging of cells in experimental disease models.* Progress in nuclear magnetic resonance spectroscopy, 2009. **55**(1): p. 61.
78. Morcos, S., *Extracellular gadolinium contrast agents: differences in stability.* European journal of radiology, 2008. **66**(2): p. 175-179.
79. Marzella, L., et al., *Safety risks with gadolinium-based contrast agents.* Journal of Magnetic Resonance Imaging: An Official Journal of the International Society for Magnetic Resonance in Medicine, 2007. **26**(3): p. 816-816.
80. Layne, K.A., et al., *Gadolinium deposition and the potential for toxicological sequelae–A literature review of issues surrounding gadolinium-based contrast agents.* British journal of clinical pharmacology, 2018. **84**(11): p. 2522-2534.
81. Mulder, W.J., et al., *Lipid-based nanoparticles for contrast-enhanced MRI and molecular imaging.* NMR in Biomedicine: An International Journal Devoted to the Development and Application of Magnetic Resonance In vivo, 2006. **19**(1): p. 142-164.
82. Nelson, K.L., et al., *Clinical safety of gadopentetate dimeglumine.* Radiology, 1995. **196**(2): p. 439-443.
83. Lin, S.P. and J.J. Brown, *MR contrast agents: physical and pharmacologic basics.* Journal of Magnetic Resonance Imaging: An Official Journal of the International Society for Magnetic Resonance in Medicine, 2007. **25**(5): p. 884-899.
84. Hood, M.N., A.D. Blankholm, and A. Stolpen, *The Rise of Off-Label Iron-Based Agents in Magnetic Resonance Imaging.* Journal of Radiology Nursing, 2019.
85. Corot, C. and D. Warlin, *Superparamagnetic iron oxide nanoparticles for MRI: contrast media pharmaceutical company R&D perspective.* Wiley Interdisciplinary Reviews: Nanomedicine and Nanobiotechnology, 2013. **5**(5): p. 411-422.

86. De León-Rodríguez, L.M., et al., *Basic MR relaxation mechanisms and contrast agent design.* Journal of Magnetic Resonance Imaging, 2015. **42**(3): p. 545-565.
87. Thakor, A.S., et al., *Clinically approved nanoparticle imaging agents.* Journal of Nuclear Medicine, 2016. **57**(12): p. 1833-1837.
88. Li, Y.-W., et al., *Superparamagnetic iron oxide-enhanced magnetic resonance imaging for focal hepatic lesions: systematic review and meta-analysis.* World Journal of Gastroenterology: WJG, 2015. **21**(14): p. 4334.
89. Napolitano, A., et al., *A new oxidation pathway of the neurotoxin 6-aminodopamine. Isolation and characterisation of a dimer with a tetrahydro [3, 4a] iminoethanophenoxazine ring system.* Tetrahedron, 1992. **48**(39): p. 8515-8522.
90. El-Faham, A. and F. Albericio, *COMU: A third generation of uronium-type coupling reagents.* Journal of peptide science: an official publication of the European Peptide Society, 2010. **16**(1): p. 6-9.
91. Mondini, S., et al., *PEBBLES and PEBBLEJUGGLER: software for accurate, unbiased, and fast measurement and analysis of nanoparticle morphology from transmission electron microscopy (TEM) micrographs.* Nanoscale, 2012. **4**(17): p. 5356-5372.
92. Linegar, K.L., et al., *Hydrodynamic radius of polyethylene glycol in solution obtained by dynamic light scattering.* Colloid journal, 2010. **72**(2): p. 279-281.
93. Lak, A., et al., *Highly stable monodisperse PEGylated iron oxide nanoparticle aqueous suspensions: a nontoxic tracer for homogeneous magnetic bioassays.* Nanoscale, 2013. **5**(23): p. 11447-11455.
94. Yang, Q., et al., *Evading immune cell uptake and clearance requires PEG grafting at densities substantially exceeding the minimum for brush conformation.* Molecular pharmaceutics, 2014. **11**(4): p. 1250-1258.
95. Schroffenegger, M., et al., *The role of chain molecular weight and hofmeister series ions in thermal aggregation of poly (2-isopropyl-2-oxazoline) grafted nanoparticles.* Polymers, 2018. **10**(4): p. 451.
96. Na, H.B., et al., *Multidentate catechol-based polyethylene glycol oligomers provide enhanced stability and biocompatibility to iron oxide nanoparticles.* ACS nano, 2012. **6**(1): p. 389-399.
97. Gal, N., *Superparamagnetic Iron Oxide Core- shell Nanoparticles; Stability and Interactions in Biological Environments.*, in *Nanobiotechnology*. 2018, BOKU.
98. Reimhult, E., *Nanoparticle interactions with blood proteins and what it means: a tutorial review.* 2019.
99. Docter, D., et al., *The nanoparticle biomolecule corona: lessons learned–challenge accepted?* Chemical Society Reviews, 2015. **44**(17): p. 6094-6121.

Appendix

A

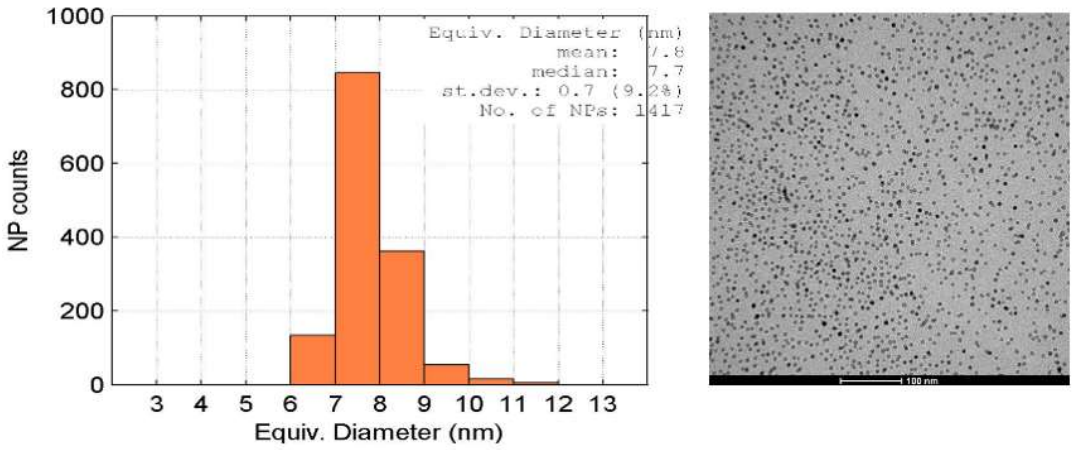

B

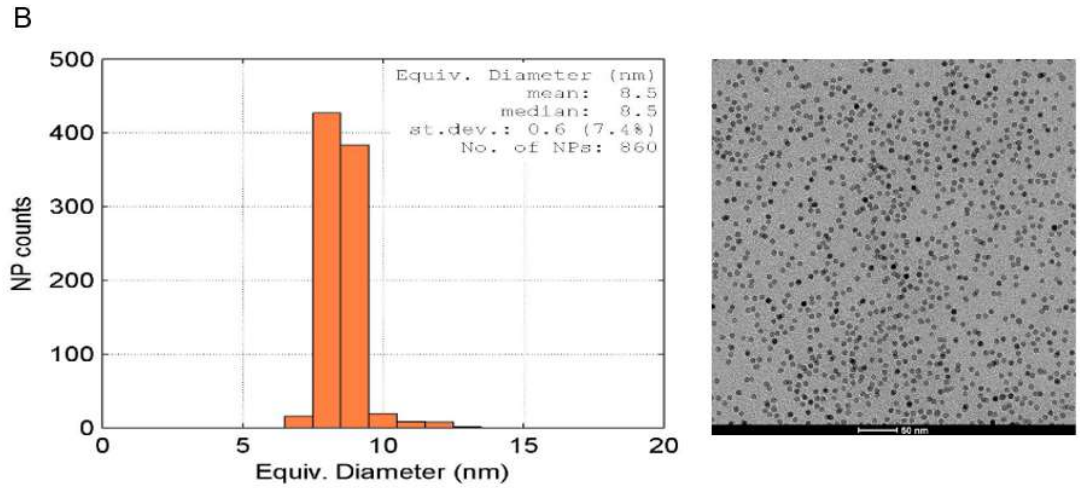

C

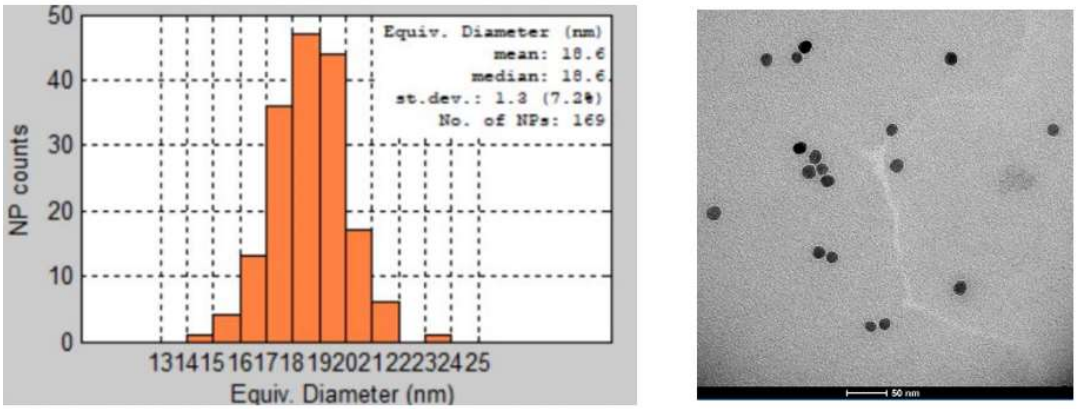

D

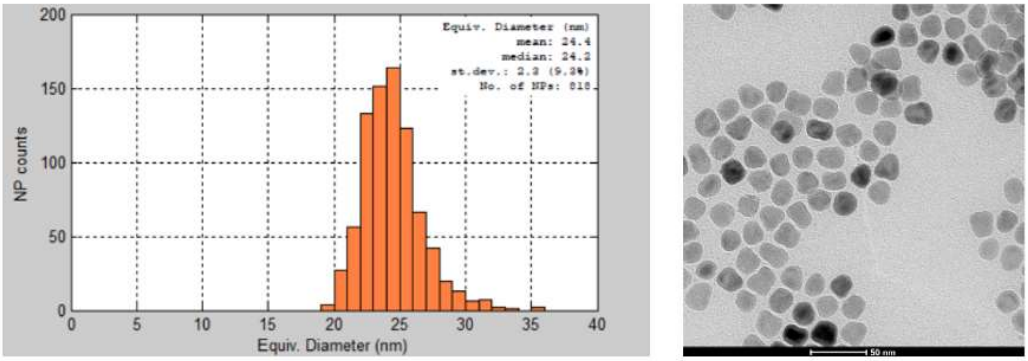

E

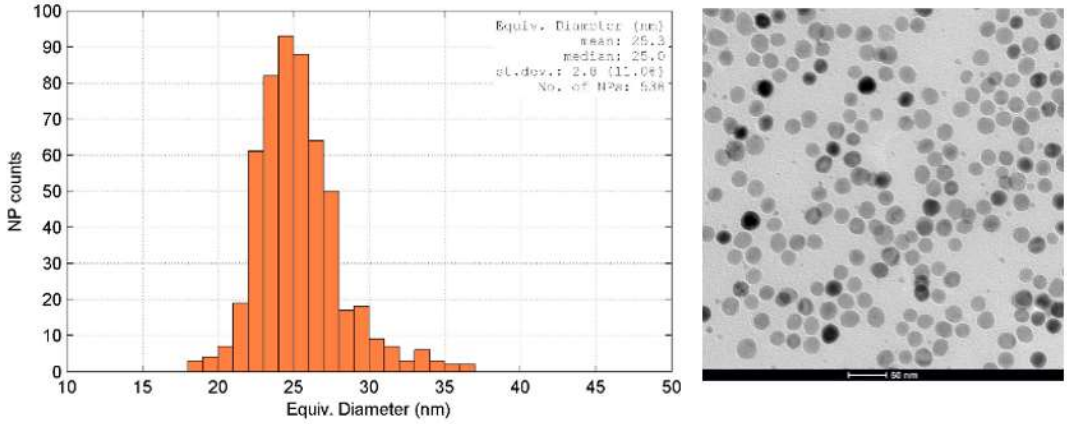

Figure 18: TEM images and size distribution graphs of extra batches of synthesised iron oxide nanoparticles which were not be involved in further experiments, A) 7.8 nm, B) 8.5 nm, C) 18.6 nm, D) 24.4 nm, E) 25.3 nm

A

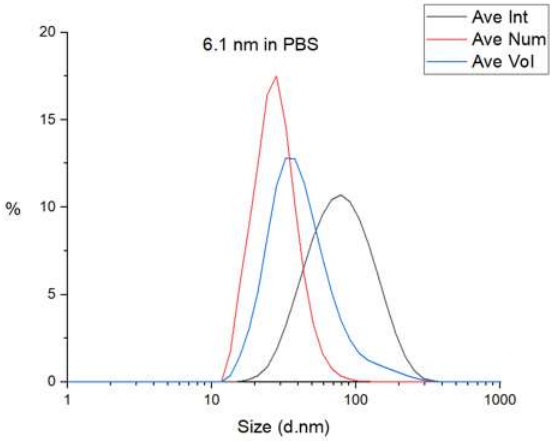
6.1 nm in PBS
Ave Int
Ave Num
Ave Vol
%
Size (d.nm)

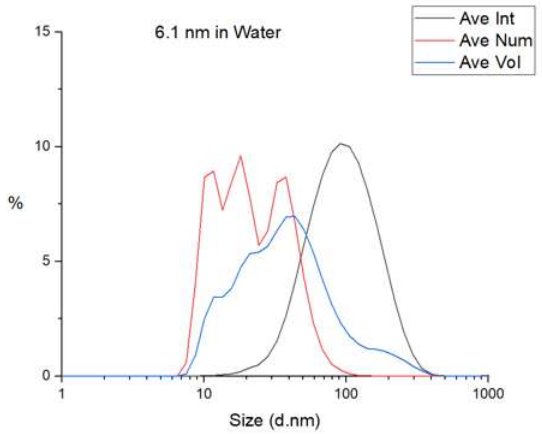
6.1 nm in Water
Ave Int
Ave Num
Ave Vol
%
Size (d.nm)

B

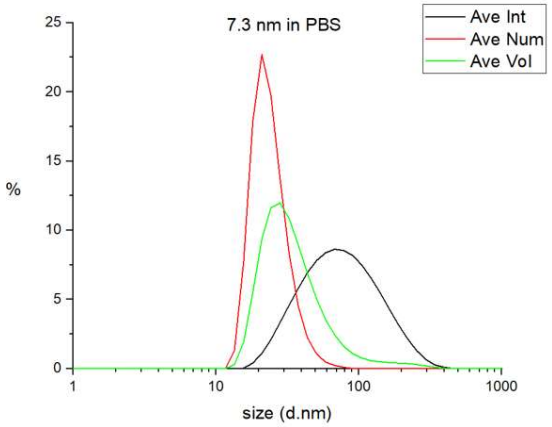
7.3 nm in PBS
Ave Int
Ave Num
Ave Vol
%
size (d.nm)

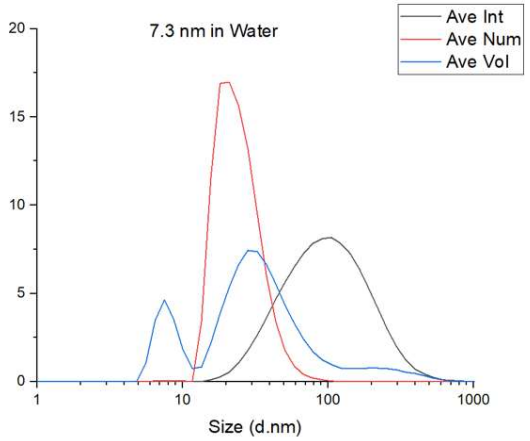
7.3 nm in Water
Ave Int
Ave Num
Ave Vol
Size (d.nm)

C

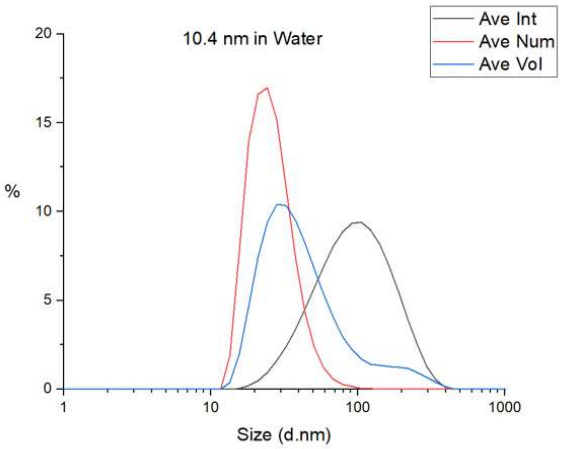
10.4 nm in Water
Ave Int
Ave Num
Ave Vol
%
Size (d.nm)

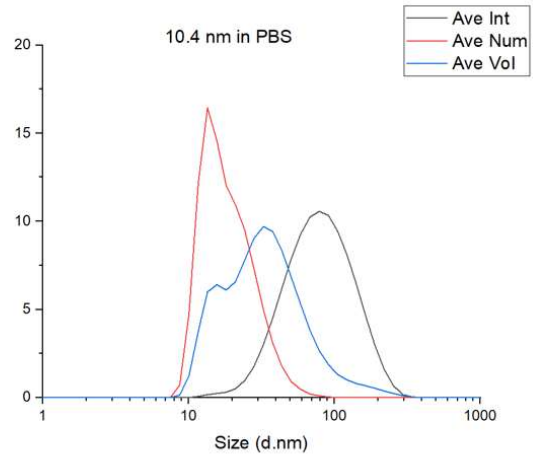
10.4 nm in PBS
Ave Int
Ave Num
Ave Vol
Size (d.nm)

c

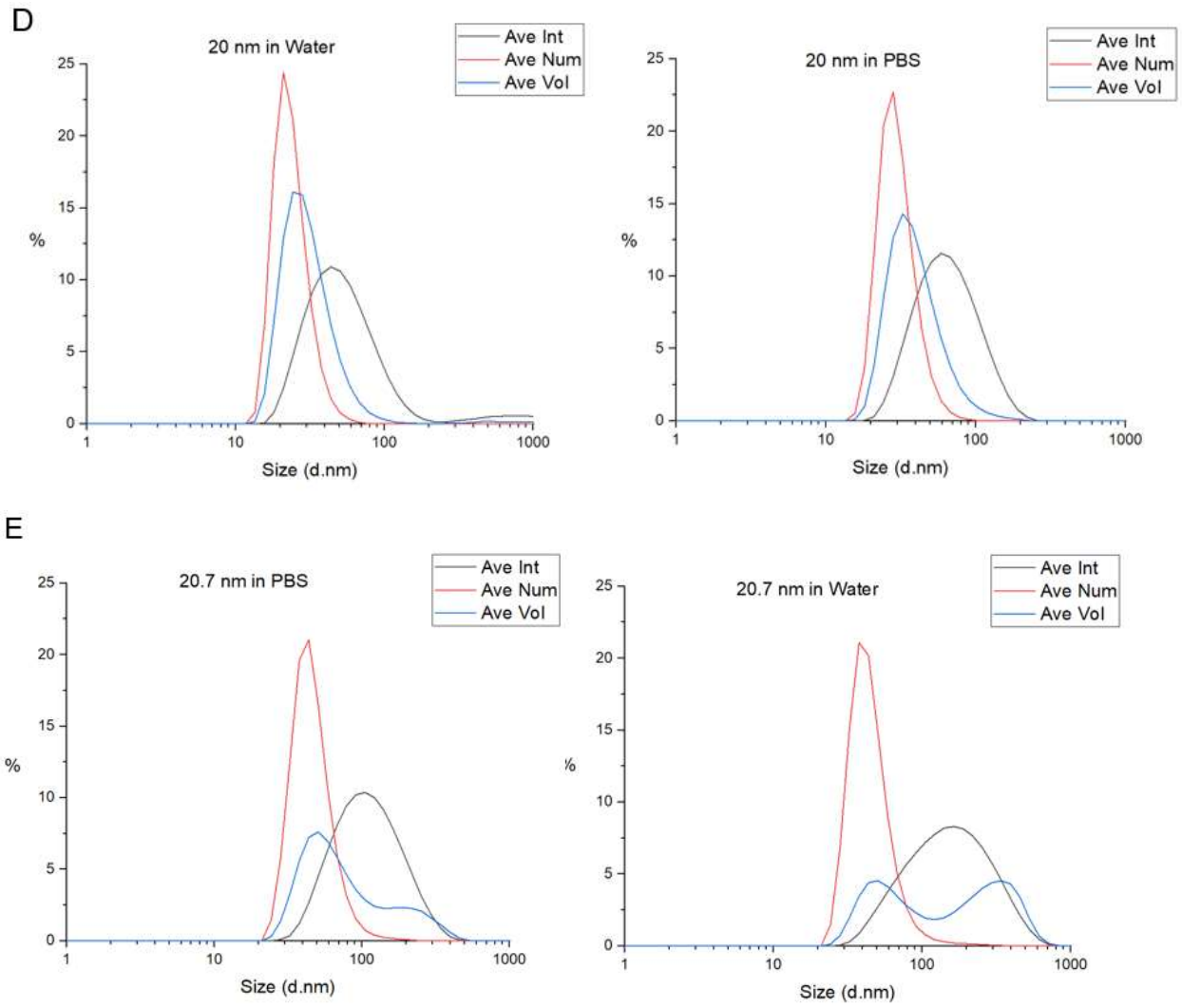

Figure 20: Hydrodynamic size distribution graphs of SPIONs functionalized by modified stripped-regrafted purified by 72h dialysis in 1000kDa membrane, derived from DLS data for SPIONs size A) 6.1 nm, B) 7.3 nm, C) 10.4 nm, D) 20 nm, E) 20.7 nm

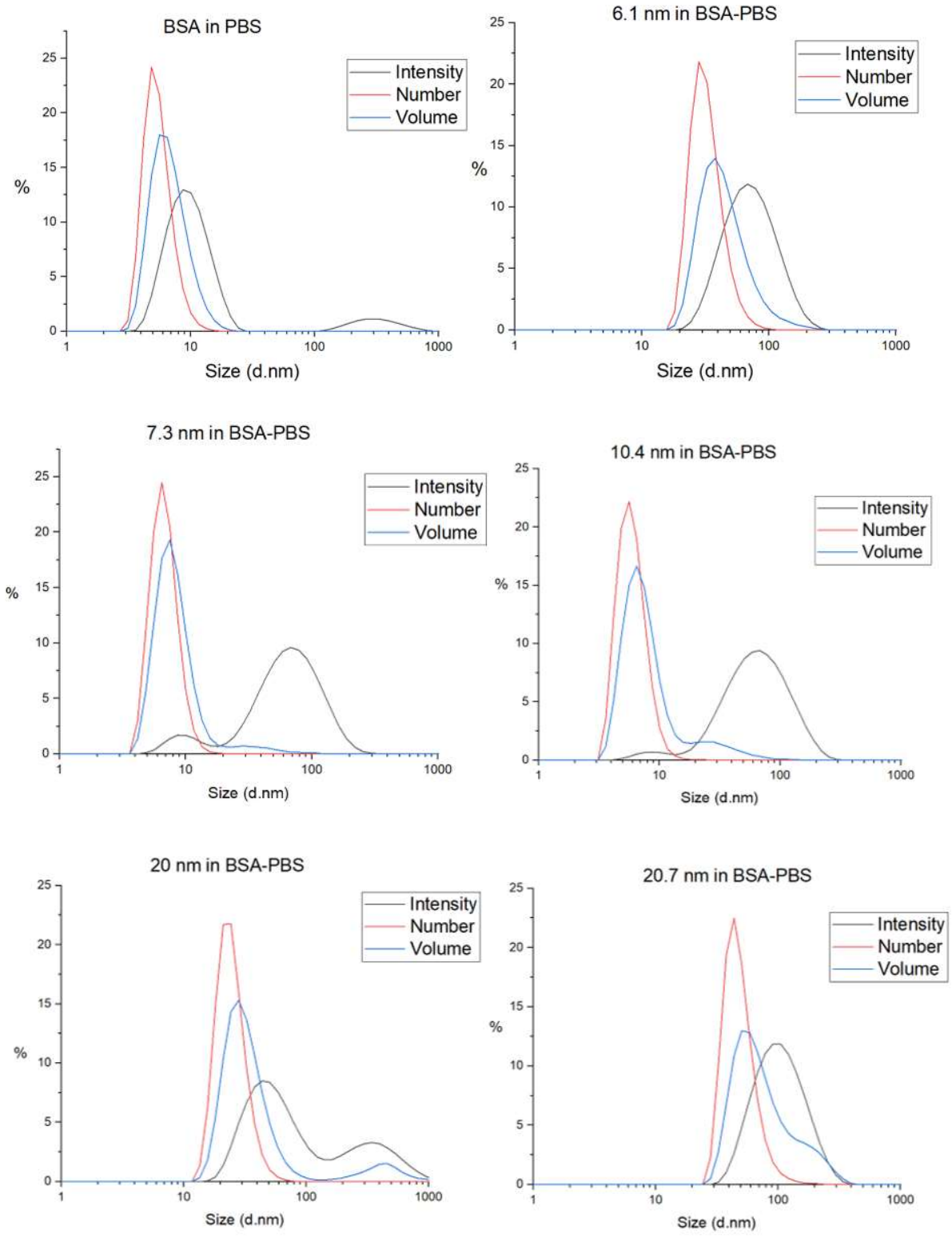

Figure 21: Protein interaction evaluation of different SPIONs sizes with Bovine Serum Albumin (BSA), investigated by DLS measurement of SPIONs after surface modification through stripping-regrafting and purification through 72 h dialysis. For SPIONs with 7.3 and 10.4 nm, signals centered on around 10 nm in intensity graphs is attributed to BSA and confirm no interaction between BSA and SPION shell.

f